

## **Sex specific role of methylcytosine dioxygenase TET1 in dopamine 1 receptor expressing medium spiny neurons in addiction.**

Haiyang Xu<sup>1,2,4</sup>, Yuxiang Li<sup>1,2,4</sup>, Qiying Ye<sup>2,3</sup>, Nicholas J. Waddell<sup>1</sup>, Amber N. Brown<sup>1</sup>, Javed M. Chitaman<sup>1,2</sup>, Graham J. Kaplan<sup>1,2</sup>, Colton E. Remedies<sup>1,2</sup>, Kristen Abreu<sup>1,2</sup>, Rachel L. Hedinger<sup>1,2</sup>, Xiaobing Zhang<sup>2,3</sup>, Peter Fraser<sup>1</sup>, Jian Feng<sup>1,2\*</sup>

<sup>1</sup>Department of Biological Science, Florida State University, Tallahassee, Florida 32306, USA.

<sup>2</sup>Program in Neuroscience, Florida State University, Tallahassee, Florida 32306, USA.

<sup>3</sup>Department of Psychology, Florida State University, Tallahassee, Florida 32306, USA.

<sup>4</sup>These authors contributed equally.

\*Corresponding author contact e-mail: [feng@bio.fsu.edu](mailto:feng@bio.fsu.edu)

### **ABSTRACT**

DNA dioxygenase Ten-eleven translocation 1 (TET1) plays essential roles in brain development and functions. In this study, we demonstrate that TET1 in dopamine D1 type receptor-expressing medium spiny neurons (D1-MSNs) sex-differentially modulates cocaine reward and addiction-like behaviors. We further reveal that TET1-dependent sex-dimorphic DNA epigenome is associated with divergent animal behavior in male and female animals. The majority of the DNA methylation changes are enriched in a novel epigenomic feature we termed Differential Methylation Hot Zones (DHZs). Using chromosome conformation capture (Hi-C), we find that some of the DHZs exhibit intertwined DNA methylation and 3D genome conformation change. Further analyses discover that sex-dimorphic DMRs and DHZs are enriched with synaptic plasticity- and neural function-related genes. With compelling evidences showing that hyperpolarization activated cyclic nucleotide gated potassium channel 1 (*Hcn1*) gene is a target of sex-dimorphic TET1 target, electrophysiologic recording confirms that the sex-dimorphism of hyperpolarization-activated current in control groups, with the differences diminishing following TET1 knock out. These findings suggest that TET1 in NAc D1-MSN is crucial in mediating the sex-differential susceptibility to the reinforcing effect of cocaine through epigenomic modulation in synaptic genes and neuronal plasticity.

## **INTRODUCTION**

Emerging evidence from both preclinical and clinical studies have unveiled the sex differences in drug addiction. For example, young adult males are prone to abuse marijuana or alcohol, while same-age females are more likely to abuse cocaine and other psychotherapeutics<sup>1</sup>. Females are also more vulnerable to the reinforcing effect of psychostimulants<sup>2,3</sup>. However, the etiology underlying this divergence remains largely unknown. It is hypothesized that dynamic interplays between innate hormones and genetic variations may contribute to the sex differences in addiction, which may be coupled together with a plausible epigenetic modulation<sup>4</sup>. This is supported by the accumulating evidence showing the association between DNA methylation, a major epigenetic mechanism, and sex differences in the brain. For example, genome wide screening suggests DNA methylation may regulate sex differences in neural function related genes<sup>5</sup>. Study in post-mortem brain tissue has identified numerous sex-differences in DNA methylation, many of which are enriched in synaptic plasticity and neural signalling pathways<sup>6</sup>. Concomitantly, DNA methyltransferase family enzymes (DNMTs), which catalyse DNA methylation, are differentially expressed between sexes in the brain during a specific time window after birth<sup>7,8</sup>. On the other hand, DNA methylation has been shown to maintain sex differences in the adult brain and behaviors, for instance, inhibition of DNMTs or conditional deletion of *Dnmt3a* elicited sexual behaviors in female rodents<sup>5,9</sup>.

Although DNA methylation has gained increasing attention on its roles in addiction<sup>10-12</sup>, whether and how it contributes to the sex difference of addiction remains unknown. In the brain, DNA methylation pattern can be established through the catalysis of DNMTs, the methylated DNA may also go through turnover via its oxidation by methylcytosine dioxygenase TET1, TET2, and TET3<sup>13</sup>. TET enzymes oxidize 5-methylcytosine (5-mC) into 5-hydroxymethylcytosine (5-hmC), which can be further converted into 5-formylcytosine (5-fC), and 5-carboxylcytosine (5-caC), in order. Therefore, DNA demethylation occurs when 5-fC and 5-caC are excised and replaced with unmethylated cytosine through thymine DNA glycosylase -mediated base excision repair<sup>14,15</sup>. TET enzymes have not only been implicated in neural gene expression, synaptic plasticity, cognition, learning and memory<sup>16-19</sup>, accumulating evidence also indicate TET's roles in addictive drug use<sup>20-22</sup>. For example, we have previously shown that TET1 in mouse nucleus accumbens (NAc) negatively mediates the rewarding effect of cocaine. With the diverse heterogeneous cell types in the brain, it remains elusive what cell type specific roles TETs play in addiction. In the NAc, the two major neuronal populations are dopamine 1 receptor - and dopamine 2 receptor - expressing medium spiny neurons (i.e., D1-MSNs and D2-MSNs), which are involved in the excitatory direct pathway and inhibitory indirect pathway, respectively<sup>23,24</sup>, and have contrasting roles in drug-induced behavioral response. For example, activation of D1-MSNs promotes motivational cocaine seeking, which may be inhibited through D2-MSN activation<sup>25,26</sup>. Therefore, it is important to further decipher out TET1's function in addiction within a defined cell type. Here, by studying the NAc D1-MSNs with integrations of mouse addiction behavioral models and whole genome DNA methylation profiling in both males and females, we found that TET1's neuron type specific function in addiction is also sex dependent, which is underlined by sex specific epigenome

changes that selectively target synaptic plasticity. Therefore, our study provides a cell type specific epigenetic insight of sex differences in addiction.

## RESULTS

### Sex-divergent roles of TET1 in D1-MSNs in cocaine addiction-like behaviors

It has been shown that TET enzymes are subjected to expression change in the brain by cocaine or morphine administration<sup>20-22,27</sup>. Overexpression of TET1 in the NAc or hippocampus attenuates cocaine reward, or voluntary morphine consumption, respectively<sup>21,22</sup>. To further address whether TET1 functions in a neuron subtype-specific manner, we generated a D1 Cre *Tet1*<sup>loxP/loxP</sup> mouse line (*Tet1* KO thereafter) to conditional knockout *Tet1* in dopamine 1 receptor expressing (Drd1) medium spiny neurons (D1-MSNs or D1 neurons, thereafter). While few has studied sex specific effects of epigenetic regulation in addiction, with the predominance of literature examined male animals in the field, we extended our work to include female mice as a variable. We found that all four groups of mice (control and *Tet1* KO mice of both sexes) were capable to develop cocaine conditioned place preference (CPP) (Fig. 1a, b). In addition, we noticed that between male and female control groups, male mice have a lower CPP score compared to the females. However, there is a sex-divergent effect of *Tet1* KO, when compared with the control mice of the same sex, with cocaine CPP being potentiated in male *Tet1* KOs and attenuated in female *Tet1* KOs. As a result, the *Tet1* deficiency in D1 neurons reverses the sex difference in cocaine CPP. Therefore, our results suggest that TET1 is implicated in the sex differences in cocaine addiction-like behaviors. TET1's sex dependent divergent roles in D1 neurons may contribute to the sex differences.

To further consolidate our findings, we examined the voluntary cocaine consumption by using operant intravenous cocaine self-administration (SA) (Fig. 1c). Under the lower-effort taking fixed ratio 1 (FR-1) test, although there was no difference for the cocaine infusion and active nose-pokes among all groups, TET1 demonstrates a sex-divergent regulation in both cocaine consumption and active nose-pokes (Fig. 1d, e), reflected by the strong interaction between *Tet1* KO and sex. Furthermore, under the higher-effort taking FR-3 schedule, an apparent sex-divergent effect of *Tet1* KO on cocaine intake and active nose pokes was observed (Fig. 1f, g). While female control mice acquired a greater number of cocaine infusions and active nose-pokes compared to the male control mice (4<sup>th</sup> and 5<sup>th</sup> day, Fig. 1f, g), *Tet1* KO displayed increased cocaine administrations in males and decreased intakes in females, in comparison to the sex-matched control mice (Fig. 1f, g). Consistently, we found a similar sex-dependent effect of TET1 on the breakpoint reached under progressive ratio (PR) schedule. Specifically, *Tet1* KO potentiated the motivation for taking cocaine in male mice, and impeded it in female mice (Fig. 1h). While male control group reached a lower breakpoint and nose poked a declined number of active holes than the female control mice, *Tet1* KO reversed this difference (Fig. 1h). Together, this is concomitant with what we found in cocaine CPP, when the opposing effects of *Tet1* KO in males and females reversed the sex difference observed in control mice.

We continued to carry out an extinction and a cue-induced reinstatement of cocaine seeking procedure to assess the continuous cocaine seeking during withdrawal and the incentive effects of the cue associated with cocaine reinforcement. We found a sex difference in extinction pattern, and a strong interaction between sex and *Tet1* KO (Extended Data Fig. 1a). Specifically, *Tet1* KO reduced the resistance to extinction of cocaine seeking in female, but enhanced the resistance in male mice. All, except the female *Tet1* KO mice, displayed robust cue-induced reinstatement of cocaine seeking (Extended data Fig. 1b), indicating TET1 affects the memory retrieval of cue-associated cocaine reinforcement in females, but not males (Extended Data Fig. 1b).

To determine whether the sex-divergent effects of *Tet1* KO in cocaine addiction can be extended to non-drug rewards, we assessed the liquid sucrose self-administration (Extended Data Fig. 2a). We found comparable sucrose infusions and active nose-pokes between *Tet1* KO and control groups in both sexes under FR-1 and FR-3, suggesting that *Tet1* KO does not affect the non-drug reinforcer's acquisition and maintenance (Extended Data Fig. 2b-e). However, for the motivation effect examined under PR schedule, TET1 showed a sex-dependent role in sucrose seeking (Extended Data Fig. 2f, g), with higher breakpoints identified in male *Tet1* KO mice, but not female KOs, in comparison to the respective sex-matched control mice (Extended Data Fig. 2f). In addition, the extinction of sucrose seeking was not affected by *Tet1* KO in either sex (Extended Data Fig. 2h). Male *Tet1* KO, in comparison to male control mice, reinstated to seek sucrose in the presence of a sucrose-related cue, reflected by more active nose-pokes (Extended Data Fig. 2i). In contrast, female *Tet1* KO mice were not able to retrieve the cue-induced reinstatement of sucrose seeking. Although *Tet1* KO mice had an enhanced reinstatement in males and an attenuated reinstatement in females, notably, we found that female control mice have a greater reinstatement than male control group. Therefore, *Tet1* deficiency reversed this sex difference to the opposite direction. Combined together, our results further support the sex divergent roles of TET1 in reward related behaviors.

### **Restoration of TET1 in nucleus accumbens D1 *Tet1* KO neurons rescued the cocaine addiction-like behavioral deficits**

Nucleus accumbens (NAc) is a key brain reward region with the vast majority neurons are medium spiny neurons, which are consist of an equal number of D1-MSNs and D2-MSNs<sup>24</sup>. To further confirm if TET1's sex specific effects in regulating addiction-like behaviors are mediated through the D1-MSNs in NAc, we expressed *Tet1* in the NAc D1 *Tet1* KO neurons. To do so, we constructed the wildtype *Tet1* catalytic domain (CD) into a Cre dependent AAV Flex-on vector (AAV2-wt*Tet1*CD-HA-EGFP) and injected it into the NAc of *Tet1* KO (D1Cre *Tet1*<sup>loxP/loxP</sup>) mice. In the control group, the AAV vector carrying the mutant *Tet1*CD (AAV2-mut*Tet1*CD-HA-EGFP) was injected into the NAc of *Tet1* KO mice. We then performed the cocaine self-administration after virus injection (Fig. 2a, Extended Data Fig. 3a, b). We found that the sex differences previously observed in male and female *Tet1* KO mice (Fig. 1d-g) were reproduced in the male and female KO groups received mutant *Tet1* injections (Fig. 2b-e). However, viral restoration of wildtype *Tet1* in NAc reversed these behavioral differences, but with opposing effects in males and females (Fig. 2b-e). There are significant interactions between sex and *Tet1* restoration on cocaine infusions and active nose pokes under both FR-1 (Fig. 2b, c) and FR-3 (Fig. 2d, e)

schedules. Furthermore, in the motivational cocaine seeking examined under the PR schedule, there was also a significant interaction between sex and *Tet1* restoration on breakpoint and active nose pokes (Fig. 2f, g). Overall, the effect of *Tet1* restoration on cocaine addiction-like behaviors is opposite to what we have observed in the *Tet1* KO, and resembles the behavioral differences between control groups of male and female in Fig. 1. Therefore, our study suggests that restoration of *Tet1* expression in the NAc D1 *Tet1* KO neurons is sufficient to rescue the effects of *Tet1* KO on cocaine administration. The contrasting behavioral changes after *Tet1* restoration in the two sexes indicates that TET1 in NAc D1-MSNs mediates the cocaine addiction-like behaviors in a sex specific manner.

### **TET1 dependent DNA methylation changes are associated with sex-specific methylome differences in nucleus accumbal D1-MSNs**

Although TET enzymes have been implicated in neural gene expression regulation, synaptic plasticity, and learning and memory<sup>18,28-30</sup>, the molecular underpinnings of TET1's function in the brain remain elusive, which particularly lack cell-type and sex-specific resolutions. To identify the genomic targets of TET1 in D1-MSNs to obtain insights of TET1's sex-specific roles in cocaine addiction-like behaviors, we examined the DNA methylome of NAc D1 *Tet1* KO neurons in both males and females. To achieve this, we generated the D1-Cre (+), *Tet1*<sup>loxP/loxP</sup>, D1-tdTomato mice with D1-Cre (-), *Tet1*<sup>loxP/loxP</sup>, D1-tdTomato as control. We isolated D1-MSNs from NAc through fluorescence-activated cell sorting (FACS). We then conducted whole-genome bisulfite sequencing (WGBS)<sup>31</sup>, with each library constructed using cells collected from a single mouse (Extended Data Fig. 4a-c, Table 1). The WGBS data demonstrated a robust correlation in global methylated CpG (mCG), as well as mCH (CH includes CA, CT and CC) levels, across all groups, indicating TET1 deficiency in D1-MSN neurons does not cause a dramatic methylome alteration (Extended Data Fig. 4d, e). In addition, we found a sex-dependant clustering when principal component analysis (PCA) was applied to autosomal mCGs across all WGBS samples (Extended Data Fig. 4f). A more robust PCA separation was observed between male and female X chromosomes (Extended Data Fig. 4f, g), which can be explained by X-chromosome inactivation, when one of the two X chromosomes in each female cell is condensed and silenced. Furthermore, we found male D1-MSNs have higher global mCG levels, no matter if the sex chromosomes are included (Fig. 3a) or not (Extended data Fig. 4h). Notably, this sex difference in global mCG levels is mitigated after *Tet1* KO (Fig. 3a, Extended data Fig. 4h).

Next, we performed the CG differentially methylated region (DMR) analysis, which include both TET1 dependent DMR analysis (i.e., ♂ *Tet1* KO vs ♂ control; ♀ *Tet1* KO vs ♀ control), and sex specific DMR analysis (i.e., ♂ control vs ♀ control; ♂ *Tet1* KO vs ♀ *Tet1* KO) (Extended Data Fig. 5a, Table 2). In each comparison, the vast majority of the DMRs are similarly situated in intronic (over 42%) or intergenic regions (over 43%), with only about 3% of DMRs located in promoter regions (Extended Data Fig. 5b). In either males or females, *Tet1* KO has more hypo-DMRs than hyper-DMRs (*Tet1* KO vs control) (red and blue bars in Fig. 3b). Meanwhile, when comparing male and female wildtype mice (♂ control vs ♀ control), the DMRs are predominately hypermethylated in males. However, *Tet1* KO abolishes this bias and leads to a more comparable overall size of hyper- and hypo-DMRs between the two sexes (♂ *Tet1* KO vs ♀ *Tet1* KO) (Fig. 3b). Among these DMRs,

the largest accumulated overlap occurred between male and female *Tet1* KO hypo-DMRs (Fig. 3b). This may reflect a sex-convergent function of TET1 in NAc D1-MSNs. Moreover, the numerous overlaps between *Tet1* dependent DMRs and sex-specific DMRs (shared DMRs between top two comparisons and bottom two comparisons in Fig. 3b) may suggest an interplay between TET1 and sex on modulating D1 neuronal methylome. In line with this, in a PCA analysis using the mCG levels of all CG DMRs, we recognized opposite trajectories of mCG alterations after *Tet1* KO in male and female D1-MSNs, in comparison to their sex-matched control, along the PC2-axis (Fig. 3c), which may reflect the sex-dependent DNA methylation changes that are associated with sex-divergent roles of *Tet1* KO in addiction-like behaviors. Furthermore, the female *Tet1* KO projects proximal to male control mice along the PC1-axis (Fig. 3c) is consistent with our observation that *Tet1* ablation may mitigate the DNA epigenomic sex differences in D1 neurons.

To obtain functional insights of the DNA methylation changes, we then performed a Gene Ontology (GO) analysis on these CG DMR associated genes (DMGs). First, we noticed the *Tet1* KO has sex dependant biological impacts ( $\sigma^{\circ}$  *Tet1* KO vs  $\sigma^{\circ}$  control;  $\varphi^{\circ}$  *Tet1* KO vs  $\varphi^{\circ}$  control) with male and female DMGs are enriched in different biological processes (Fig. 3d). These enrichments are all associated with hypo DMRs, but not hyper DMRs, which are fewer in number than hypo DMRs in each of the two comparisons. Additionally, there are profound GO terms enriched in hyper DMRs in control males vs control females comparison, which is nearly abolished after *Tet1* KO ( $\sigma^{\circ}$  *Tet1* KO vs  $\varphi^{\circ}$  *Tet1* KO) (Fig. 3d). Remarkably, genes related to neural function, particularly synaptic transmission, are predominantly enriched in these GOs.

One major aspect of the regulatory role of DNA methylation in gene transcription is its interaction with transcription factors (TFs)<sup>32,33</sup>. Analysis of TF binding motifs at the DMRs revealed the enrichment of numerous TFs' binding sites, which mostly belong to a handful of TF families (Fig. 3e). Among them, a few (e.g., Mef2<sup>34-36</sup>) are known for their implications in neuronal activity and addictions. Notably, activator protein-1 (AP-1) TF family binding sites are selectively enriched in both male *Tet1* KO hypo-DMRs ( $\sigma^{\circ}$  *Tet1* KO vs  $\sigma^{\circ}$  control) and sex-dependent hyper-DMRs ( $\sigma^{\circ}$  control vs  $\varphi^{\circ}$  control), the same groups of DMRs that have most neural function-related GO term enrichments (Fig. 3d). In the AP-1 complex, FosB is a component whose truncked form TF ( $\Delta$ FosB) has been implicated in lasting neural and behavioral plasticity in drug addiction<sup>37</sup>. Using a published  $\Delta$ FosB ChIP-seq dataset in NAc D1-MSNs<sup>38</sup>, we found that the enrichment of  $\Delta$ FosB to the genomic target sites is negatively correlated with the DNA methylation levels (Extended Data Fig. 5c). Therefore, the TET1 dependent differential enrichment of TF binding motifs in D1-MSN DMRs between males and females (Fig. 3e) may represent a molecular underpinning of the sex specific role of TET1 in addiction.

We further applied K-means clustering to examine the DNA methylation dynamics across all D1-MSN CG DMRs in control and *Tet1* KO mice of both sexes. While a portion (cluster 5) demonstrated a convergent hypomethylation after *Tet1* KO independent of sex, the majority of CG DMRs exhibited varying degrees of sex specificity (Fig. 3f).

Taken together, our results suggest that in NAc D1 neurons, TET1 mediates the sex differences in DNA methylation, which may contribute to the sex specific modulations of neuronal function in addiction.

### **TET1 dependent differential methylation changes cluster in hot zones**

Notably, in the K-means clustering analysis, we found multiple clusters of DMRs are located predominantly within the same chromosome (arrowheads in Fig. 3f), which suggests a genomic positional effect of TET1 dependent DNA methylation changes. In addition, we noticed high densities of DMRs that are concentrated to certain genomic regions (Extended Data Fig. 5a). To obtain a more detailed view with CpG site resolution, we plotted the distribution of CG differentially methylated loci (DMLs) along each chromosome and observed a similar feature (Fig. 4a-c): where high-density same direction differential methylation changes distributed along a long stretch of genomic region (tens of kilobases to several megabases). For the ease of communication, we call them as “Differential Methylation Hot Zone” or DHZ (Extended Data Fig. 5d). Based on the density of CG hyper- or hypo- DMLs in genomic bins, we identified 264 CG DHZs (Table 7). These DHZs accommodate the majority (~82.5%) of CG DMLs and over half (~58%) of the CG DMRs (Extended Data Fig. 5e). For example, on chromosome 8 (chr 8), there are a few DHZs with high densities of *Tet1* KO dependent hypo-DMLs in megabase-long regions that appear to be consistent in both sexes (“sex-convergent” TET1-dependent DHZs, Fig. 4a, b). Meanwhile, some *Tet1* dependent DHZs have opposite directions of DNA methylation changes in males and females, such as on chr14 and chr17 (“sex-divergent” TET1-dependent DHZs, Fig. 4a, c). Furthermore, we found the individual CpG sites located in the same DHZ usually have the same direction of methylation changes (Extended Data Fig. 5f). This is exemplified by both the sex-convergent DHZ on chr8 (Fig. 4b, d), where the entire zone region displayed hypomethylation in both male and female *Tet1* KOs, and the sex-divergent DHZ on chr14 (Fig. 4c, e), with hypomethylation throughout the DHZ region in male *Tet1* KO and hypermethylation in female *Tet1* KO. The opposite DNA methylation changes in male and female *Tet1* KOs also abolished CG methylation differences observed in the chr14 DHZ between male and female controls (Fig. 4c, e). Furthermore, even though in sex-divergent DHZs the methylation changes are in opposite directions in males and females, these DHZs usually share the same boundaries in both sexes. In addition, the boundaries of *Tet1* dependent DHZs often coincide with that of sex-specific DHZs detected from the ♂ control vs ♀ control comparison (Fig 4c). This further supports our notion of TET1’s pivotal role in establishing sex-specific DNA methylome in D1 neurons.

As TET1 also shows an activity at non-CG (CH) sites in the brain<sup>28</sup>, we then extended our methylation analysis to CH DMLs. In the comparisons between male KO vs male Con, female KO vs female Con, and male KO vs female KO, we identified more CH hyper-DMLs than CH hypo-DMLs and these CH hyper-DMLs are predominantly (94.5% and 94.7% respectively) located in CG hypo-DHZs (Fig. 4b, c, Extended Data Fig. 5g). However, in the male Con vs female Con comparison, more CH hypo-DMLs were recognized which are mostly overlapped with CG hyper-DHZs (Extended Data Fig. 5g). Further analysis indicates a high correlation for the co-occurrence between CG hypo-DMLs and CH hyper-DMLs, or between CG hyper-DMLs and CH hypo-DMLs

(Extended Data Fig. 5h). Therefore, our results recognize DHZ as a genomic feature of TET1-dependant DNA methylation changes, which may have sex-specificity and contrasting patterns between CG and non-CG methylations.

We further characterized NAc MSN cell type-specific DHZs by comparing the male control D1-MSN methylomes generated from this study with our previously published methylomes of male mice D2-MSNs<sup>31</sup>, the other major neuron type in NAc that have contrasting roles in addiction NAc. Remarkably, we identified widespread cell type-specific CG DMLs/DHZs (Table 8) and overlaying CH (represented by CA) DMLs, with the vast majority of them have opposite directions of methylation changes (Extended Data Fig. 6a, b). This suggests that DHZ may be a common feature of neuronal methylome in NAc. In addition, we found a small portion of overlapping CG DHZs and CH DMLs that have the same direction of methylation changes (Extended Data Fig. 6b). Among them, in D1-MSN vs D2-MSN comparison, D1 marker genes (e.g., *Drd1*, *Pdyn*) are hypomethylated in their genic region CG DMLs and CH DMLs (Fig. 4f, Extended Data Fig. 6c), whereas the D2 marker genes, (e.g., *Drd2*, *Adora2a*) are hypermethylated in their DHZs (Fig. 4g, Extended Data Fig. 6c). From this, we speculate that the presence of DHZs with convergent CG and CH methylation change may represent a more stable cell type specific epigenetic state, whereas the DHZs with divergent CG and CH methylation alterations may reflect a labile epigenetic state that is more widespread in D1 neuronal methylome.

### **TET1 dependent DNA methylation changes are associated with higher order genome organization alterations**

Mammalian genomes are organized in a complex and hierarchical three-dimensional (3D) manner that usually encompass megabases of DNA sequences<sup>39-43</sup>. Given that the DHZs span a long stretch of DNA with clear boundaries and the coordinated TET1 dependent DNA methylation change at chromosome levels (Fig. 3f), we postulated that TET1 may be engaged into higher order genome organization. Thus, we performed chromosome conformation capture (Hi-C) assay<sup>42</sup> to examine the 3D genome architecture in NAc D1 *Tet1* KO neurons (Table 9, Extended Data Fig. 7a). The consistency of the Hi-C assay was validated by pairwise correlation analysis of all replicates across all autosomes (SCC correlation score > 0.96) (Fig. 5a). In addition, we found a clear separation by sex on the X chromosome analysis (Fig. 5a). Independent from genotype, X chromosome pairwise correlations show higher scores in same sex comparisons and lower correlation scores (< 0.96) in male vs female comparisons, and therefore separated into two clusters (Fig. 5a). This may be explained by the X chromosome inactivation in females. We should note that due to the inability to differentiate the DNA sequences between inactivated and activated X chromosomes in females, we cannot rule out the possibility that the lower correlation between male and female X chromosomes is due to any sex-difference that is independent of X inactivation. Furthermore, among all autosomes, chr 8 has the most dramatic 3D changes with its SCC correlation scores clearly impacted by genotype (*Tet1* KO/Con), but not sex difference. Chr 8 sample pairs of the same genotype in either sex share similar higher SCC scores, compared with the lower SCC scores of comparisons from different genotypes (Fig 5a, b). This suggests that TET1 impacts 3D genome organization changes that is more prominent in certain chromosome. Notably, further examination revealed that *Tet1* KO decreased chromosome interactions in a ~10

Mbp area on chr8, which aligned with the aforementioned sex-convergent hypomethylated-DHZ (Fig. 4b, Fig. 5c). The effect appears to be comparable between males and females (Fig. 5c). By conducting a differential analysis of individual Hi-C replicates, we found numerous differential interaction regions (DIRs) that include one falls into this chr 8 region (Fig. 5d). Furthermore, we found that DIR can also be associated with a sex-divergent DHZ. For example, a DIR with reduced interactions is located at the sex-divergent DHZ on chromosome 14 (Fig. 4c, Fig. 5c, Table 10), but only in the male *Tet1* KO vs male control comparison, in which DHZ is hypomethylated. No such DIR is recognized in the female *Tet1* KO vs female control comparison, when the DHZ is hypermethylated.

Following the observation of DNA hypomethylation (DHZ) associated with alterations in the 3D genome structure (DIR), we conducted a detailed analysis of the ensuing chromosome conformation changes in these hot zones. The 3D genome is partitioned into A and B compartments, with A compartment encompasses with actively transcribed, gene-rich regions, and more compact, silenced genomic regions are enclosed in B compartment<sup>42</sup>. We found that TET1-dependent DIRs (compare *Tet1* KO vs control of the same sex) are all located in B compartments with elevated PC1 values, which indicates compromised compartmentalization (Extended Data Fig. 7b). Concurrently, we found the 3D chromatin loop interactions<sup>44</sup> within the TET1-dependent DIRs in chr 8 are significantly decreased (Extended Data Fig. 7c). Furthermore, we identified multiple sex-specific DIRs when comparing male and female Hi-C replicates from the same genotype (Fig. 5d). We found they all overlapped with the sex-specific DHZs (Extended Data Fig. 7d). Moreover, these sex-specific DIRs are only detectable in the male and female control comparison, but not in the male vs female *Tet1* KO comparison (Fig. 5d). This further indicates that the sex difference in 3D genome organization is attenuated after *Tet1* KO, an observation reminiscent of our findings in the DNA methylome analysis, and addiction-like behaviors. Together, we found 3D organization changes may represent an additional layer of TET1 mediated epigenomic modulation that is closely associated with DHZs.

### Sex specific roles of TET1 in D1-MSN synaptic plasticity

Next, we continued to explore the functional roles of TET1-dependent epigenomic changes in NAc D1 neurons. We found that CG DMRs were significantly enriched in the genomic anchors of Hi-C loops (Extended Data Fig. 8a), which supports an integrated effect of TET1 on DNA methylation and chromatin looping. We then defined *Tet1* KO CG DMR-associated genes (DMGs) by assigning CG DMRs to both linear nearby genes and genes connected by 3D chromatin loops (Extended Data Fig. 8b), and analyzed the sex-convergent DMGs (cluster 5 in Fig. 3f, where DNA methylation change in *Tet1* KO is consistent between sexes) and sex-dimorphic DMGs (the ones linked to sex-specific DMRs, which include all clusters other than cluster 5 in Fig. 3f), respectively. Notably, while no significant pathway enrichment was found in sex-convergent DMGs, sex-dimorphic DMGs are highly enriched with various neural function related pathways (Fig. 6a), that is consistent with our findings of TET1's sex specific roles in brain function. For example, in one enrichment pathway of "amphetamine addiction" (Fig. 6a, b), there are multiple genes that are broadly involved in addiction. Among their DMRs, a few (e.g., *Gria1*, *Cacna1c*, *Ppp3ca*, *Camk2b*) demonstrated a main effect of sex on DNA methylation, when there are same directions of

methylation changes in male control vs female control and male *Tet1* KO vs female *Tet1* KO comparisons. Multiple others (e.g., *Grin2b*, *Ppp3cc*, *Camk2d*, *Calm1*, and *Creb3l1*) exhibit an effect of sex-TET1 interaction, with frequent hypo-methylation observed in male *Tet1* KO vs male control comparisons, whereas the direction of methylation change at the same gene is reversed or abolished in female *Tet1* KO when compared to female control. Together, this suggests a TET1-dependent epigenetic similarities and disparities between sexes in the brain, which may be associated with addiction.

As the majority of DMRs are located in DHZs (Extended Data Fig. 5e), to obtain further insights of DHZ's functional implication, we compared the GO terms enriched by DMGs with DMRs located within DHZ, outside of DHZ, and genes with Hi-C loops fall inside a DHZ. We found that all three groups of genes are mostly enriched with synaptic function related GO terms (Fig. 6c). Most of these synaptic genes' methylation changes are influenced by sex, TET1, or sex-TET1 interaction (Fig. 6d). For example, in addition to its CG DMRs (Fig. 6b), the entire *Grin2b* gene's DNA methylation level is also under a significant effect of sex-TET1 interaction (Fig. 6d, Extended Data Fig. 8c). *Grin2b* is a glutamate receptor that plays crucial roles in synaptic transmission and plasticity. In control mice, there are higher mCG levels in males than females. However, *Tet1* KO led to hypomethylation in males and hypermethylation in females. Thus, the sex difference in DNA methylation of *Grin2b* gene is reversed due to *Tet1* KO's opposite effects on methylation change in males and females (Extended Data Fig. 8c, d). Notably, the *Grin2b* gene locus occupies a 3D hierarchical genome interaction architecture within a 4-Mb DHZ (Extended Data Fig. 8d). Thus, the *Grin2b* CG DMRs appear to fluctuate synergistically across the DHZ, which representing two levels of DNA methylation regulation (Extended Data Fig. 8d). Furthermore, we also found an interesting effect between sex and TET1 in *Hcn1* (hyperpolarization activated cyclic nucleotide gated potassium channel 1), a gene encodes an ion channel protein that is crucial for hyperpolarization-activated current ( $I_h$ ) and plays important roles in neuronal excitability. Intersecting with the *Hcn1* gene locus, we found a 385-kb DHZ displayed higher CG methylation in control males than females (Fig. 6e, f). However, *Tet1* knockout leads to methylation decrease in males and increase in females. Though the combined effect of *Tet1* knockout is not sufficient to reverse the methylation pattern as happens in *Grin2b*, it attenuated the sex difference in DNA methylation of *Hcn1* (Fig. 6e, f). Furthermore, we identified a promoter-proximal 3D genomic loop of *Hcn1* was a differentially interacting loop (Fig. 6g, Table 14), which was strengthened after *Tet1*-KO only in females. Though the function of *Hcn1* in addiction remains unknown, it indicates that *Hcn1* in the estrogen receptor 2-expressing neurons of bed nucleus of the stria terminalis may mediate the sexual satiety in a male specific manner<sup>45</sup>. Thus, the TET1 dependent epigenomic signature provides insights of sex-specific roles of *Hcn1* that deserves further investigation.

We then determined whether *Tet1* KO induces electrophysiological property changes in NAc D1-MSNs. To study the intrinsic excitability of D1-MSNs in NAc, we monitored the resting membrane potential and the action potential evoked by current injections using current-clamp recordings in brain slices (Fig. 6h). Compared to control mice of the same sex, NAc core D1-MSNs of *Tet1* KO mice had significantly hyperpolarized resting membrane potentials in both males and females (Fig. 6i), suggesting TET1's sex independent role in the control of resting

membrane potential of D1-MSNs. We further found that both the amplitudes of the threshold and the saturated current injection for evoking action potential of NAc D1-MSNs were significantly higher in female KO in comparison to female control but were not significantly different between male *Tet1* KO and control mice (Fig. 6j, k), which suggests a sex difference of TET1 in regulating neuronal excitability. We then examined spontaneous excitatory postsynaptic currents (sEPSCs) when membrane potentials were held at -70 mV. We found the sEPSC frequency of NAc D1-MSNs was higher in female KO mice than that of female control, while no obvious difference was observed between two male groups (Fig. 6l). However, we detected little difference in sEPSC amplitude among all groups (Fig. 6m). With our finding of TET1 dependent epigenetic regulation of *Hcn1* that is also sex-specific (Fig. 6e-g), we examined whether hyperpolarization-evoked currents ( $I_h$ ) of NAc D1-MSNs were altered in *Tet1* KO in both sexes. Therefore, we recorded  $I_h$  in NAc core D1-MSNs of slices using hyperpolarizing voltage pulses of 1s from -40 to -150 mV in steps of 10 mV (Fig. 6n). In male mice, we did not observe significant difference in  $I_h$  amplitude between *Tet1* KO and control mice (Fig. 6p). However, female control mice showed a smaller  $I_h$  currents which were partially recovered by *Tet1* KO (Fig. 6o).

Therefore, our results provide compelling evidence that TET1 regulates epigenetic changes and electrophysiological property differences in NAc D1-MSNs in a sex-specific manner, which may underline the sex-dependent drug addiction-like behaviors. To further assess the TET1 targeted genes that could regulate addiction-like behaviors, we compiled genes exhibiting either DNA methylation or 3D chromosomal interaction alterations in our datasets. Then we integrate this list with two previously reported addiction-related gene lists: one consisting of D1-MSN addiction-associated genes identified through genome-wide association studies<sup>46</sup>, and another comprising NAc addiction index genes, whose transcription levels in NAc have been correlated with mouse cocaine addiction behaviors<sup>47</sup> (Extended Data Fig. 9a, Table 15). Among them, the top-ranked genes include *Grin2b* and *Hcn1*, as described above, and many others, with some have documented implications in addiction. For example, *Auts2* was reported to mediate cocaine addictive behaviors in mice that is subjected to both DNA methylation modulations and 3D looping with adjacent gene *Calm1*<sup>48</sup>. Our study shows that two DHZ-like regions in *Auts2* and *Calm1* loci exhibit concordant TET1-dependent changes in CG methylation (Extended Data Fig. 9b). Furthermore, these two DHZs exhibit genome interaction in a “stripe” structure<sup>49</sup>, a type of chromosomal configuration in which one genomic locus interacting with a consecutive genomic target region. Though most of other candidate genes’ functions in addiction remains unexplored, they may serve as a repertoire of novel candidates for future efforts to obtain molecular insights of neuron subtype dependent, sex specific epigenetic regulation of addiction.

## Discussion

Despite the various evidence of sex differences in addiction, little is known about the underlying neurobiological mechanisms. Our findings indicated a prominent sex-difference in the role of TET1 within NAc D1-MSNs in regulating cocaine reward and addiction-like behaviors. Male control mice demonstrated a naturally lower cocaine preference, numbers of cocaine intake and active responses and lower motivation for taking cocaine compared with their female control littermates, which were consistent with previous reports in rats<sup>50-52</sup>. However, few studies have

been executed upon investigating the sex difference in cocaine addiction-like behavior in mice. A recent report has revealed that female mice self-administered slightly more cocaine under FR-1 schedule and earned a higher breakpoint under PR with lower dose of cocaine (0.3 mg/kg/infusion) compared with those measured in their male counterparts, despite no difference observed under a higher cocaine dose (1 mg/kg/infusion)<sup>53</sup>. In this current study, under more effort-taking schedules (FR-3 and PR), we observed even stronger sex difference of control mice in cocaine intake with a comparable lower cocaine dose (0.5 mg/kg/infusion). TET1 in D1 neurons sex-divergently regulates acquisition and maintenance for cocaine but not sucrose SA. However, TET1 has profound and consistent effects on the retrieval of both cocaine- and sucrose-related memories reflected by the cue-induced reinstatement test of reinforcer seeking, especially in female mice which are even more vulnerable to *Tet1* KO. The consistent role of TET1 in regulating memory retrieval suggests the shared neurobiological mechanisms of DNA demethylation in regulating drug- and natural reward-associated memories. In fact, all four groups of mice acquired and maintained a stable and comparable sucrose SA paradigm, which ruled out a potential learning deficiency for operant response in *Tet1* KO mouse. Further, restoration of wild-type but not mutant mouse *Tet1* CD affected the behavioral pattern between male *Tet1* KO and female *Tet1* KO mice, corroborating that the TET1 enzymatic activity was indispensable for the TET1's role in D1-MSN. Collectively, NAc D1-MSN-derived *Tet1* plays a critical role in cocaine addiction in a sex-specific manner.

TET1 serves as a fundamental component in the DNA methylation dynamics, and its expression is responsive to neuronal activity and found to be dysregulated in response to stress and drugs of abuse<sup>18,22,29,54</sup>. Our neuronal subtype-specific investigation substantiated repeatedly reported sex differences in cocaine usage in laboratory animals<sup>4,50,51,55</sup>, and discovered notable sex-divergent addiction-related ramifications following *Tet1* knockout. Further high-resolution DNA methylation studies have revealed behavior-correlated DNA methylation in CG DMRs, where the binding affinity of AP-1/FosB transcription factors and associated genes in related neuronal processes might be differentially regulated.

It has been reported TET1 deficient induced hypomethylation in heterochromatic genomic compartment in cancer cells<sup>56</sup>. Here in postmitotic neurons, we recognized DHZs as CG DML/DMR hot zones, most of which are characterized by pervasive loss of CG methylation and gain of sporadic CH methylation post *Tet1* KO. The mCH level of genes within neurons has been demonstrated to inversely correlate with gene expression<sup>57</sup>. Brain tissue-specific study also shows that mCH DMRs were highly associated with differential gene expression<sup>58</sup>. The concurrent presence of CG hypo-methylation and CH hyper-methylation in DHZs might act either synergistically or counterbalance the epigenomic alterations induced by TET1. Our data present a snapshot of the dynamics of DNA methylation, and further studies are required to elucidate the functional implications of these opposing shifts in CG and CH methylation.

Similar to DMRs, the DHZs are predominantly Sex-specific and TET1-dependent on a much larger genomic scale. The detection of sex-specific DHZs comparing males to females of control groups suggests a role for TET1 in establishing and maintaining epigenomic sex differences. Intriguingly, we also identified cell subtype-specific (NAc D1-MSN vs NAc D2-MSN) DHZs, which implies

neuronal subtype-specific roles of TET1 in D1-MSN and D2-MSN. In light of this, we conducted a cocaine SA test using mouse lines with conditional *Tet1* KO in D2 neurons. Although extensive literature has documented the distinct roles of D1- and D2-MSNs in drug-induced behavioral responses, there is no report to date, to our best knowledge, that examines the role of DNA methylation or demethylation in these two neuronal subpopulations synchronously in drug addiction. The results indicated that *Tet1* KO in D2-receptor expressing neurons did not affect cocaine addiction-like behavior at any phase in males, while potentiated cocaine intake in females (data not shown), opposite with the role of D1-MSN-sourced TET1 in regulating cocaine reinforcement in female in this current report. Therefore, these results highlighted that the regulation of TET1 is both sex- and neuron subtype-specific.

We explored the association between DHZs and genome organization. There are emerging links between DNA methylation and 3D genome architecture<sup>56,59</sup>. Integrative analysis of DNA methylation and genome conformation demonstrates that *Tet1* KO leads to 3D genome organization alteration, most drastically at the DHZ on chromosome 8. Interestingly, a recent study reported that mouse chromosome 8 in mouse neurons undergoes notable 3D genome reorganization during the progression of neurodegeneration, accompanied by DNA damage accumulation<sup>60</sup>. This suggests that TET1 and potential common genome 3D architectures (of chr8) may underpin the 3D genome organization change observed in these two pathologies. Notably, the restoration experiment using only the TET1 catalytic domain (TET1CD) resulted in reversed sex difference in SA infusion and nose-poke activity. This implies TET1CD, despite lacking the DNA binding motif, retained at least a portion of its genomic localization preferences, a finding consistent with previous studies on different TET1 isoforms<sup>30,61</sup>. It is therefore tempting to hypothesize that genome organization facilitates the enrichment of TET1 proximate to DHZs. In addition, sex-specific DIRs existed only in control groups but were absent in *Tet1* KO groups, thus supporting the interplay between TET1 and sex in the regulation of 3D genome organization. Accumulating evidence suggests that DNA methylation causally regulates genome organization<sup>62,63</sup>. However, the intricate mechanisms underlying the interplay between CG, CH methylation, and genome organization alteration in DHZs still warrant further exploration.

Synaptic genes are significantly associated with sex- and TET1-specific epigenomic alterations. This functional implication of sex- and TET1-dependent DNA epigenomic variation is solidified by the sex- and TET1-specific electrophysiologic traits. Although the enrichment of both sex- and *Tet1*-dependent DMR genes within synaptic plasticity-related GO terms (Fig. 6c), the resting membrane potentials, the threshold and saturated stimulus required for evoking an action potential, as well as the sEPSCs in NAc D1-MSNs do not differ between male control and female control mice, which is in line with the previous report<sup>64</sup>. It has been documented that DNA methylation homeostasis regulates neuronal intrinsic membrane excitability<sup>65</sup>. Our data also revealed that TET1 is required for the control of resting membrane potentials in NAc D1-MSNs regardless of sex, whereas female D1-MSNs are more vulnerable to TET1-regulated neuronal excitability. Further, the hyperpolarization evoked ( $I_h$ ) currents by various steps of voltage vary among four groups, and highly correlate with the difference patterns of mCG level of DHZ overlapping *hcni* locus, i.e., *Tet1* KO attenuates the magnitude of difference observed in female and male Control mice. Meanwhile, significant alterations of  $I_h$  currents in *Tet1* KO female but not male mice echoed

the changes in the chromatin interaction of *hcn1* Hi-C loops in female KO mice. HCN channels are activated by membrane hyperpolarization and are permeable to Na<sup>+</sup> and K<sup>+</sup>. These channels play major role in controlling neuronal excitability and synaptic transmission and involve the mechanisms of synaptic plasticity and memory<sup>66</sup>. The current findings in the I<sub>h</sub> cation current by the HCN channels suggest that *hcn1* and its downstream activities may constitute one of the core mechanisms underlying the sex differences of TET1 in regulation cocaine reward and addiction-like behaviors. However, the physiology of D1-MSN neurons most likely results from the allostasis of multiple interacting synaptic networks rather than from any single gene/protein.

Biological sex differences are mainly attributed to disparate sex hormones, sex chromosomes, and epigenomic mechanisms<sup>4,8</sup>. An increasing body of evidence emphasizes the role of DNA methylation in establishing and maintenance of sex differences<sup>9,67</sup>. Our mouse model is controlled for genetic variation and the behavior-correlated epigenomic alteration in this study are all located in the autosomes, which provide compelling evidence for the contribution of epigenomic regulation of TET1 to sex differences in a neuronal subtype. It further implies that the sex hormones may interact with Tet1 in the establishment of the sex-specific epigenome. Due to technical limitations, we excluded sex chromosomes from most of our analysis, which represents a limitation that should be addressed in future studies. Nevertheless, the prominence of the sex-specific facet of TET1 regulation reaffirms the importance of considering the factor of sex in research<sup>68,69</sup>. Our study pinpointed the sex-divergent ramification of Tet1 deficiency in a neuronal subtype and provided molecular evidence for sex differences in reward and drug addiction, supporting the idea that DNA methylation and 3D genome organization are important underlying mechanisms for neuropsychiatric disorders.

## Methods

### Animals

All mice used in this study were born and raised in a temperature controlled laboratory condition at 12-hour reverse light/dark lighting cycle (6:00 to 18:00 dark hours). Pups were housed with their dams after being born and weaned at postnatal day 21, after which they were group housed by sex with ad libitum access to food and water. All mice used in this study were in C57BL/6J genetic background and were at least 8 weeks of age, unless otherwise noted. All experiments followed the guidelines of the Animal Care and Use Committee of Florida State University.

### Generation of *Tet1* conditioned knockout mice

*Tet1*<sup>loxP/loxP</sup> mice<sup>54,70,71</sup> were crossed with *Drd1-Cre* (*D1-Cre* thereafter)<sup>72</sup> heterozygous mice to generate *D1-Cre(+)*; *Tet1*<sup>loxP/+</sup> mice, which were then mated with *Tet1*<sup>loxP/loxP</sup> mice to generate *D1-Cre(+)*; *Tet1*<sup>loxP/loxP</sup> mice. The strain was expanded by breeding *Tet1*<sup>loxP/loxP</sup> mice with *D1-Cre(+)*; *Tet1*<sup>loxP/loxP</sup> mice. The offspring *D1-Cre(+)*; *Tet1*<sup>loxP/loxP</sup> and *D1-Cre(-)*; *Tet1*<sup>loxP/loxP</sup> were used as *Tet1* KO and control, respectively.

## Generation of *Tet1* conditioned knockout reporter mice

*D1-tdTomato*<sup>73</sup> heterozygous mice were crossed with *Tet1*<sup>loxP/loxP</sup> to generate *Tet1*<sup>loxP/+</sup>; *D1-tdTomato* mice, which were then bred with *Tet1*<sup>loxP/loxP</sup> to generate *Tet1*<sup>loxP/loxP</sup>; *D1-tdTomato* mice. The *Tet1*<sup>loxP/loxP</sup>; *D1-tdTomato* mice were then crossed with *D1-Cre(+)*; *Tet1*<sup>loxP/loxP</sup> to derive progeny of *D1-Cre(+)*; *Tet1*<sup>loxP/loxP</sup>; *D1-tdTomato* and *Tet1*<sup>loxP/loxP</sup>; *D1-tdTomato* that were used in FACS to isolate *Tet1* KO and control D1-neurons, respectively.

## Genotyping PCR

Mouse ear punch was used for DNA isolation and PCR genotyping<sup>54</sup>. Briefly, ear tissue samples were digested with 500 µL TENS buffer (20 mM Tris-HCl (pH 8.0), 1 mM EDTA (pH 8.0), 400 mM NaCl, 1% SDS) and Proteinase K (final concentration: 0.5 mg/mL, VWR, Suwanee, GA) at 55 °C overnight. The samples were then incubated at 37 °C for 30 mins with 0.5 ug RNase A added (Thermo Fisher, EN0531, Waltham, MA, USA). DNA was purified by phenol-chloriform (VWR, #97064-694, Suwanee, GA, USA ) and dissolved in TE, which was then used for genotyping PCR, with the PCR primers listed in Table 16.

## Adeno-associated virus (AAV) preparation and brain stereotaxic injection

The mouse *Tet1* catalytic domain coding sequence (CD of TET1 amino acids 1367-2039) and the mutant *Tet1* catalytic domain (*mutTet1CD*: same sequence as TET1CD, except with two point mutations at H1652Y, D1654A) were retrieved as previously reported<sup>13</sup>. By using the FLEX-on design, we reversely inserted the *HA-wtTet1CD* or *HA-mutTet1CD* fusion downstream to a CMV promoter in between interlocking pairs of lox 2272 and loxP sites, to generate the *Tet1* wildtype and *Tet1* mutant constructs, respectively. An *EGFP* coding sequence was added outside of the loxP sites for expression inspection (Extended Data Fig. 3a). The designed vectors were synthesized and packed into Adeno-associated virus 2 (AAV2) by VectorBuilder Inc (Santa Clara, CA, USA).

Bilateral nucleus accumbens (NAc) micro-injections were performed as previously reported<sup>74</sup>. Briefly, mice were anesthetized with a mixture of xylazine (10 mg/kg) and ketamine (90 mg/kg), positioned in a mouse stereotaxic station, and the skull was exposed. To target the NAc bilaterally, Hamilton syringe needles (33 g) (at a 10° angle) were positioned to +1.6 mm (AP), ±1.5 mm (ML), and -4.4 mm (DV). A volume of 0.5 µl of virus was infused into NAc of each side at a rate of 0.1 µl/min over a 5-min period followed by a 5-min of rest. The injection sites were confirmed by EGFP expression observed under a fluorescence stereomicroscope using brain slices following the completion of the behavioral test.

## Immunohistochemistry validation of viral expression

Equal volume (0.5 µL) of AAV-*wtTet1CD* and AAV-*mutTet1CD* were injected into left and right NAc of the same mouse, respectively. Mice were perfused with 4% paraformaldehyde using a peristaltic pump 21 days after the viral injection. The brain was removed and postfixed in 4% PFA overnight at 4 °C, followed by dehydration using gradient sucrose (20% followed by 30% sucrose in 0.01 M PBS, pH 7.4). Then the brain was sliced into 12 µm sections using a cryostat (Leica

Biosystems, Buffalo Grove, IL). The brain sections containing NAc were used for immunofluorescent validation analysis. Briefly, after 1 hour of blocking in PBS solution containing 5% goat normal serum and 1% BSA, brain sections were incubated with rabbit anti-HA primary antibody (1: 250; ab9110, Abcam, Cambridge, MA, USA) for 24 hours in a humidified chamber at 4 °C. Next, the sections were incubated with Alexa Fluor 555 goat anti-rabbit secondary antibody (1: 500, A-21428, Life Technologies, Grand Island, NY, USA) for 2 hours at RT. The DAPI staining was applied for counter-staining. Slides were visualized under a Nikon CSU-W1 confocal microscope (Nikon Instruments Inc., Melville, NY, USA). The viral infected neurons were visualized by EGFP fluorescence, and the viral infected D1 medium spiny neurons were confirmed by HA staining(Extended Data Fig. 3b).

### Cocaine conditioned place preference (CPP)

Mice were trained in an unbiased three-compartment conditioned place preference apparatus, as described previously<sup>74</sup>. During habituation, control and *Tet1* KO mice were placed in the center chamber and allowed to explore freely in all compartments for 10 min. In the 20 min pretest session, which was carried out the next day after habituation, the animals were placed into the central chamber to allow free movement among all three compartments with time spent in each compartment recorded. Mice spent more than 70% of the total trial time in one side were excluded from experiment. Mice were then subjected to conditioning sessions in the following two consecutive days, when mice received i.p. injections of saline (10 ml/kg) in the morning session in the saline-paired compartment and cocaine (10 mg/kg in 1 mg/ml concentration) in the afternoon session in the opposite side of compartment (drug-paired). Each conditioning session lasted for 30 min. A post-test session identical to the pre-test was conducted on the following day after the last conditioning session. The place preference score was determined as the difference between time spent in the drug-paired compartment and the time in the saline-paired compartment.

### Intravenous cocaine self-administration

#### Instrumental response

Control and *Tet1* KO mice were used for initial sucrose training by using standard mouse self-administration chambers (Med Associates Inc., Albans, VT, USA)<sup>74</sup>. Each chamber has a house light and two nose-poke holes (one active nose-poke hole with 2 cue lights located inside and above the hole, respectively and one inactive nose-poke hole). Operant training was conducted with 10% sucrose solution in a daily 2-hour session under a fixed ratio 1 schedule (FR-1), when one nose-poke of the active hole resulted in one delivery of sucrose solution (12 µl/ 2 seconds) to the liquid receptacle. This was followed by a 20-sec time-out period, when the cue lights were on and the house light was off, with no sucrose delivery. The nose pokes during the time-out were also recorded. The criteria for the establishment of equipment response were set at 40 sucrose infusions in each of two consecutive sessions, and at least 80% discrimination of the active nose-poke hole. The maximum liquid sucrose reward was set at 100 infusions in one session. After FR-1, one session FR-3 (i.e., three active responses are required to obtain one infusion of sucrose solution) schedule was carried out. For the groups of mice that obtained stereotaxic injection of AAV, the sucrose training was performed eight days after the stereotaxic surgery.

### Jugular vein catheterization surgery

The jugular vein catheterization surgery was done after completion of instrumental response training . Mice were anesthetized with a mixture of xylazine (10 mg/kg) and ketamine (90 mg/kg). An indwelling catheter (26 G stainless steel with a 5-mm length pedestal) connected with a 6 cm silicone tubing was implanted into the right jugular vein, and the catheter base was mounted on the back of the animal. The catheter was flushed with 0.02 mL heparinized (30 IU/mL) saline containing antibiotics and was sealed and locked with a plastic dummy cannula. Catheter was flushed daily with heparin (30 IU/mL) in sterile normal saline with antibiotics during the recovery period (4 days), after which catheter was flushed daily using heparin only (30 IU/mL) until completion of cocaine self-administration.

### Acquisition and maintenance of intravenous cocaine self-administration

All self-administration experiments were carried out one session per day. Each mouse was placed in a self-administration chamber with the back-mounted catheter connected to a cocaine delivery syringe mounted on an infusion pump. Active nose-pokes resulted in an infusion of 19  $\mu$ L cocaine delivered over 3 seconds. Cocaine infusions were coupled with simultaneous illumination of the cue lights and extinguishing of the house light, followed by a 20-sec time-out period; during which, nose-pokes were recorded, but no programmed drug infusion was given. The total daily drug intake was limited to 30 mg/kg/day. Mice were trained for cocaine self-administration in 2-h daily sessions to acquire operant responding maintained by cocaine (0.5 mg/kg/infusion, i.v.) under 7-day FR-1 and the following 5-day FR-3 schedule. The criteria for acquisition of operant responding were set when mice maintained stable responding with less than 20% deviation from the mean of the total number of infusions earned in three consecutive sessions, with at least 80% responding on the active nose-poke, and a minimum of 12 reinforcements per session.

To further determine the motivation for cocaine intake, one day after the last session under FR-3, animals were tested one time under the progressive ratio (PR) schedule, when the number of active response required to earn the cocaine reinforcer escalated. The duration of the PR session was 3 hours maximum or until mice did not acquire infusion within 1 hour. The breakpoint and active nose-pokes were recorded. "Breakpoint" was defined as the last completed ratio to acquire cocaine infusion. After the PR session, an infusion of ketamine (20  $\mu$ L, 15 mg/mL) was administered through the catheter, and only mice that displayed catheter patency (i.e., mice manifested the symptom of ataxia within 3 seconds following ketamine infusion) were advanced to the extinction and cue-induced reinstatement tests .

### Extinction of operant responding and cue-induced re-instatement of cocaine seeking

Mice were forwarded to extinction phase 24 hours after PR testing. Mice experienced a 2-hour extinction session per day for 10 consecutive days, during which cocaine and the cocaine-associated cue light were unavailable, and nose-poking was recorded but with no consequence. The criteria for extinction were met when the number of active responses was less than 25 per session during three consecutive sessions. One day after the last extinction session, mice were examined for a session of reinstatement test. Cue-induced reinstatement of cocaine seeking was conducted under the same conditions used in the acquisition phase, except that no cocaine was delivered following an active nose-poke. However, the syringe pump was still operating when animals poked the active hole. The reinstatement criterion was set when the number of active responses doubled compared to that made during the last extinction session.

## **Oral sucrose self-administration, extinction, and cue-induced reinstatement of sucrose seeking**

Following instrument response/sucrose self-administration, control and *Tet1* KO mice were used for sucrose self-administration assessment. The timeline of acquisition and maintenance of sucrose self-administration were identical to that of cocaine self-administration. The maximum number of 10% sucrose reinforcer was set at 100 infusions in a 2-h session. All mice were subjected to 5 days of extinction test followed by one session of cue-induced reinstatement of sucrose seeking behavioral test one day after extinction.

### **Statistical analyses for behavioral tests**

All behavioral data were analysed by two- or three-way analysis of variance (ANOVA) or three-way repeated-measures ANOVA using Graphpad Prism software (Graphpad Prism 9, Boston, MA, USA). Significant main or interaction effects were examined followed by Newman-Keuls *post hoc* comparision as appropriate. The criterion for significance was set at  $p < 0.05$ .

### **Electrophysiology brain slice preparation and patch-clamp recording**

Coronal brain slices (300  $\mu\text{m}$  thick) containing NAc were prepared from both *Tet1*<sup>loxP/loxP</sup>; *D1-tdTomato* (as control) and *D1-Cre(+)*; *Tet1*<sup>loxP/loxP</sup>; *D1-tdTomato* (as *Tet1* KO) mice of 4- to 8-week-old. For whole-cell recording of NAc D1-MSNs, brain slices were transferred to a recording chamber mounted on a Zeiss upright microscope (Zeiss, Berlin, Germany) and perfused with a continuous flow of gassed artificial cerebrospinal fluid (ACSF) solution containing (in mM) 124 NaCl, 3 KCl, 2 MgCl<sub>2</sub>, 2 CaCl<sub>2</sub>, 1.23 NaH<sub>2</sub>PO<sub>4</sub>, 26 NaHCO<sub>3</sub>, and 10 glucose (bubbled with 95% O<sub>2</sub>/5% CO<sub>2</sub>; 300–305 mOsm). Pipettes used for whole-cell recording had resistances ranging from 5 to 8 M $\Omega$  when filled with K-gluconate pipette solution containing (in mM) 145 potassium gluconate, 1 MgCl<sub>2</sub>, 10 HEPES, 1.1 EGTA, 2 Mg-ATP, 0.5 Na<sub>2</sub>-GTP, and 5 disodium phosphocreatine (pH 7.3 with KOH; 290–295 mOsm) or KCl pipette solution containing 145 KCl, 1 MgCl<sub>2</sub>, 10 HEPES, 1.1 EGTA, 2 Mg-ATP, 0.5 Na<sub>2</sub>-GTP, and 5 disodium phosphocreatine (pH 7.3 with KOH; 290–295 mOsm). EPC-10 patch-clamp amplifier (HEKA Instruments, NY, USA) and PatchMaster 2x90.5 software (HEKA Elektronik, Lambrecht/Pfalz, Germany) were used to acquire and analyze the data. To decrease the variance of neuronal diversity, we selectively identified and recorded medial NAc core neurons in the brain slices visible by tdTomato fluorescence expression under microscope.

For current-clamp recording, action potentials were evoked firing by current steps from 10 to 300 pA. The current threshold was defined as the injected current that evoked the first action potential. The saturated current stimulation was defined as the smallest injected current that evoked maximal frequency of action potentials.

For voltage-clamp recording, the membrane potentials were held at -70 mV for recording spontaneous synaptic currents. Traces were processed using Igor Pro 6.37 (Wavemetrics, OR, USA). Spontaneous postsynaptic currents were analyzed using MiniAnalysis 6.03 (Synaptosoft Inc., GA, USA). To evoke hyperpolarization-evoked currents (I<sub>h</sub>), the membrane potentials were

first held at -40 mV for 1 s and then switched to various levels for 1 s ranging from -150 to -40 mV in steps of 10 mV followed by a duration of 1 s at -70 mV.

All electrophysiological data were analysed by either two-way ANOVA or three-way repeated measures ANOVA followed by Bonferroni multiple post hoc comparison.

### **Isolation of NAc *Tet1* KO D1-MSNs**

One-millimeter-thick coronary brain section containing NAc region was harvested from *Tet1*<sup>loxP/loxP</sup>; *D1-tdTomato* (control), or *D1-Cre* (+); *Tet1*<sup>loxP/loxP</sup>; *D1-tdTomato* (*Tet1* KO) mouse using an ice cold stainless steel mouse brain matrix. NAc tissue was punched out using a 14-gauge stainless steel blunt tip needle and minced into small pieces using razor blades in ice cold Hibernate A minus calcium medium (Brainbits, #HACA500, Springfield, IL, USA) plus 0.25% (v/v) GlutaMAX (Thermo Fisher Scientific, #35050079, Waltham, MA, USA) and 2% (v/v) B27 supplement (Fisher Scientific, #17504044, Waltham, MA, USA). Then, the minced tissue was transferred to Hibernate A minus calcium medium with 20 unit/mL papain (Worthington, #LK003176, Lakewood, NJ, USA), 5% trehalose (Acros organics, #AC30987, Geel, Belgium), 0.25% (v/v) GlutaMAX, and 0.1 mg/mL DNase (Worthington, #LK003170, Lakewood, NJ, USA) for digestion at 37 °C for 30 min with 700 rpm agitation. The sample was then washed briefly with Hibernate A minus calcium medium with 0.25% (v/v) GlutaMAX, 2% (v/v) B27 and 1% BSA, and triturated to cell suspension by using 18g and 22g needles successively. After passing through a 70 µm cell strainer, the cells were sorted using a FACS Aria SORP instrument (BD Biosciences, USA) using a 100 µm nozzle. Cells with appropriate size and granularity were identified by gating on SSC-H and FSC-H (Extended Data Figure 4a, b). The tdTomato positive D1 neurons were isolated by fluorescence signals of 561-582/15-A (red) and 488-530/30-A (green) and collected in ice-cold 1xPBS buffer supplemented with 1% BSA.

### **DNA/RNA extraction**

Each genomic DNA sample was extracted from FACS-sorted D1-MSNs in NAc of a single animal using AllPrep DNA/RNA Micro Kit (Qiagen, #80284, Hilden, Nordrhein-Westfalen, Germany) by following the kit protocol. Sorted cells were pelleted with 500g for 5 min and the supernatant was removed. The cells were then lysed using 350 µl RLT plus buffer supplemented with 1%(v/v) of 2-Mercaptoethanol. The lysate was passed through the AllPrep DNA spin column to continue the DNA isolation, with the flow-through saved for RNA extraction. The DNA column was washed sequentially with 500 µl AW1 and 500 AW2 with 13x000g centrifugation for 1 min. Afterwards, the column was centrifuged at 13,000g for 2 min to dry up. 30 µl 70 °C preheated Elution buffer was applied onto the center of the column and incubated at room temperature (RT) for 5 min. The genomic DNA was collected by centrifugation for 1 minute. For RNA extraction, 350 µl 70% ethanol was added to the saved DNA column flow-through. After thorough mixing, it was transferred to an RNeasy MinElute spin column. Wash the column sequentially with 700 µl Buffer RW1, 500 ul Buffer RPE, and 500 ul freshly prepared 80% ethanol with centrifugation at 13,000g for 1 minute for each wash step. Finally, place the Rneasy column on a new 2 ml tube and centrifuge at 13,000 for 5 min to dry up and elute the RNA in 15 µl of RNase-free water.

## Real-time PCR

The extracted RNA was reverse-transcribed into cDNA using the qScript<sup>TM</sup> cDNA SuperMix (QuantaBio, #95048, Beverly, Massachusetts, USA). PerfeCTa SYBR<sup>®</sup> Green SuperMix was used for realtime PCR reactions. PCR primers targeting D1-MSN marker genes (*Drd1*, *Pdyn*), D2-MSN marker genes (*Drd2*, *Gpr6*), and the astrocyte marker gene (*Gfap*) were employed to confirm the identity and purity of the sorted cells. Gene expression levels were normalized to *Gapdh*. The sequences of all primers employed are provided in Table 16.

## Whole-genome DNA methylation sequencing

### Library preparation

Whole-genome bisulfite sequencing (WGBS) libraries were prepared as previously reported.<sup>31</sup> Each WGBS library was prepared from one DNA sample originating from a single mouse (n = 6 for male control, n = 5 for male KO, n = 5 for female control, n = 6 for female KO). For each sample, 40 ng of D1-MSN DNA was combined with 4 pg unmethylated lambda spike-in DNA (Promega, #D1521, Madison, WI, USA). It was then fragmented to an average size of 350 base pairs using a Covaris E220 (Covaris, Woburn, MA, USA). The fragmented DNA samples underwent bisulfite conversion using EZ DNA Methylation Gold Kits (Zymo, #D5005, Irvine, CA, USA). 20ul fragmented DNA was treated with 130 µl CT Conversion Reagent (98 °C 10 min, 64 °C 2.5 hours, 4 °C hold). The bisulfite reaction solution was loaded to IC column with 600 µl M-Binding buffer added. After one round of wash of 100 µl M-Wash buffer, the on-column desulphonation was performed with 200µl M-Desulphonation buffer at RT for 15 min. Afer desulphonation, the column was centrifuged and washed twice with 200 µl M-washing buffer, then the reslulting single-stranded DNA was eluted in 15 µl M-Elution buffer. This bisulfite converted DNA was used for library preparation using the Accel-NGS Methyl-Seq DNA Library Kit (Swift, #30024, Ann Arbor, MI, USA). For library preparation, 15 µl DNA was denatured at 95 °C for 2 min and then placed on ice imediately for 2 min. 25 µl Adaptase mix was added in and incubated at 37 °C for 15 min. Next, 44 µl extension mix was added to perform the extension reaction (98 °C 1 minute, 62 °C 2 min, 65 °C 5 min, and held at 4 °C). The resulting DNA was purified with 1.2X volume of SPRIselect beads (Beckman Coulter, #B23317, Indianapolis, IN, USA) and resuspended with 15 ul low-EDTA TE buffer. Together with 15 µl ligation mix, the ligation reaction was performed (25 °C 15 min) and the resultant DNA was purified with 1X volume of SPRIselect beads, PCR-amplified for 7 cycles, and the final library was purified using 0.85 volume of SPRIselect beads. These WGBS libraries, including 20% spike-in, were pooled and sequenced with 100bp paired-end mode on a Novaseq 6000 platform (Illumina, San Diego, CA, USA).

### Whole genome bisulfite sequencing data processing

FASTQ files of whole genome bisulfite sequencing data were generated by the Illumina analysis pipeline. Paired-end reads were trimmed with an additional 15 base pairs (bp) from 5' ends and 4 bp from 3' ends after adaptor-trimming using Trim Galore 0.6.4 ([https://www.bioinformatics.babraham.ac.uk/projects/trim\\_galore/](https://www.bioinformatics.babraham.ac.uk/projects/trim_galore/)) and Cutadapt 1.18<sup>75</sup>. Sequencing reads with low-quality (Phred quality score < 20) or shorter than 20 bp were also removed. The bisulfite conversion efficiency was assessed by aligning processed reads to the reference sequence of lambda DNA (J02459.1). All samples had a CG conversion rate of over

99.74%. The CA, CC, and CT conversion rates were also estimated using unmethylated lambda DNA as a reference. Processed read pairs were aligned to the mm10 mouse genome (for male samples) or mm10 mouse genome without the Y chromosome (for female samples), by Bismark<sup>76</sup> and Bowtie2<sup>77</sup> using “bismark --bowtie2 --gzip -X 1000 --parallel 4 --bam”. The reference genome includes autosomes, sex chromosomes, and mitochondria, but with non-chromosomal contigs excluded. After de-duplication and removal of non-conversion reads, the methylation base call with genomic context information was generated by Bismark using “bismark\_methylation\_extractor -p --bedGraph --gzip --parallel 8 --CX --cytosine\_report”. The detailed summary of WGBS library sequencing parameters is available in Table 1. The “multiBigwigSummary bins” of Deeptools 3.5.0<sup>78</sup> was used for methylation level profiling and whole-genome correlation analysis with default setting (10 kb binsize). The functions “bedtools makewindows” and “bedtool map” of Bedtools v2.30.0<sup>79</sup> was used to calculate the mCG levels in 100 kb bins of autosomes or X chromosome for the principle component analysis.

#### CG differential methylation analysis

Differential methylation analyses were performed for TET1-dependent differences (i.e., male *Tet1* KO vs. male control, and female *Tet1* KO vs. female control), and sex-specific differences (i.e., male control vs. female control, and male *Tet1* KO vs. female *Tet1* KO), respectively. CG differentially methylated loci (DMLs) and differentially methylated regions (DMRs) were performed in R using DSS<sup>80</sup> with 100 bp smoothing window<sup>81</sup> on strand-merged CG methylation data. The CpG site was only included in differential analysis if its coverage was no less than 5 in at least three replicates within the comparison. Otherwise, it will be excluded from differential analysis. The CpG sites that passed this criterion were used to estimate the effective genome size covered by WGBS experiments. DMLs were identified with a methylation β value alteration threshold of 5% and a p-value threshold of 10<sup>-4</sup>. The DMRs were identified using a 10<sup>-3</sup> p-value threshold and at least 3 CpG sites. Sex chromosomes were included in comparisons between *Tet1* KO and control groups within the same sex, and excluded from the male vs. female methylation comparisons. The ΔFosB ChIP-seq from male mice D1-MSNs was retrieved from a previous publication (GEO:GSE197668)<sup>38</sup>. The average DNA methylation levels at high, middle, and low groups of ΔFosB binding sites ( $\pm$ 1000 bp) were visualized using “computeMatrix reference-point --binSize 50 -b 2000 -a 2000” and “plotProfile” of Deeptools.

#### DMR associated genes annotation, functional enrichment and transcription factor motif enrichment analysis

Annotation of DMRs to DMR associated genes (DMGs) was performed using “annotatePeak” function of ChIPseeker<sup>82</sup> with reference of mouse genome annotation “org.Mm.eg.db”(DOI: 10.18129/B9.bioc.org.Mm.eg.db). The “compareCluster” function of ClusterProfiler<sup>83</sup> was used for the DMGs Gene Ontology and Kyoto Encyclopedia of Genes and Genomes (KEGG) pathway enrichment and comparison analyses. The enriched GO terms and KEGG pathways passed the threshold of p-value less than 0.05 after mulitple-comparison correction were presented. “findMotifsGenome.pl mm10r -size given -len 6,8,12,16” of HOMER<sup>84</sup> tool kit was used to profile the enrichment of transcription factor motifs within CG DMRs.

#### K-mean clustering of D1-MSN DMRs

To perform the K-mean cluster of D1-MSN DMRs, we merged the overlapping DMRs from four comparisons, which reduced the 2622 D1-MSN DMRs (Table 2) to 2,130 unique DMRs. The raw mCG and unmethylated CG counts of these 2,130 CG DMRs were used to calculate the mCG level of each DMR in each replicate. R package ComplexHeatmap<sup>85</sup> was used to cluster D1-MSN DMRs. The mCG levels are center-normalized and DMRs were clustered based on Euclidean distance using “centroid” algorithm. We tested cluster numbers (K) from 5 to 20 and chose K = 12 based on the result of an elbow examination.

#### Identification of Differential Methylation Hot Zones (DHZs)

To identify the Differential Methylation Hot Zone (or DHZs), we initially used DSS to detect CG DMLs from four comparisons using DSS on strand-merged methylation data without smoothing. Only CpG sites with coverage of at least 10 in a minimum of three replicates were included. The threshold of 5% methylation  $\beta$  value and  $10^{-2}$  p-value was applied. We then quantified CG DMLs within 10 kb windows with 5 kb sliding bins across the mouse genome covered by bisulfite sequencing. Next, the p-value for each bin was calculated under the hypothesis that the number of DMLs in each 10-kb window follows a Poisson distribution, using the average numbers of DML across genomic bins as the expected mean for Poisson distribution. Subsequently, p-values of all bins were aggregated by Comb-p<sup>86</sup>. Resulting regions exceeding 20 kb with p-values less than  $10^{-10}$  were defined as DHZs. For a few regions ( $n = 1$  for female *Tet1* KO vs. Con hyper-DHZs,  $n = 3$  for Con male vs. female hypo-DHZs,  $n = 1$  for *Tet1* KO male vs. female hyper-DHZs) that were identified as both hyper- and hypo-DHZ regions due to high numbers of both hyper- and hypo-DMLs, we manually classified them as hyper- or hypo-DHZ based on the predominant existing changes (hypermethylation or hypomethylation) in each region. To visualize the methylation changes in multiple scales near DHZs and genes inside DHZs, we calculated and visualized DNA methylation changes across 51 resolutions ranging from 1 kb to 20 Mb using customized scripts.

#### Non-CG differentially methylated loci analysis

Methylated CH sites at 1% FDR was identified using a binomial test considering the conversion rate inferred by unmethylated lambda spike-in as previously reported<sup>87</sup>. DSS was then used on all methylated CH sites which passed the binomial test to perform the CH differential analysis. Similar to the CpG differential analysis, a CpH site was only included in differential analysis if it had a coverage of at least 5 in a minimum of three replicates of each group. The methylation  $\beta$  value alteration threshold of 5% and p-value threshold of  $10^{-4}$  were applied.

#### Identification of NAc MSN cell-type specific CG and non-CG DMLs and DHZs

To explore the cell-type specific DNA methylation change, we compared six male D1-MSN control WGBS replicates from this study to four D2-MSN male methylomes (two WGBS and two EM-seq replicates) that we previously published (GSE195752)<sup>31</sup>. Given that methylation difference between different MSN cell types are greater than those between four D1-MSN groups, we identified the D1-MSN vs D2-MSN CG DMLs with methylation  $\beta$  value alteration threshold of 20% and p-value threshold of  $10^{-4}$ . Additionally, we identified non-CG CA DML (because the majority of non-CG methylation is at CA sites) with methylation  $\beta$  value alteration threshold of 10% and p-value threshold of  $10^{-4}$ . Cell type-specific Differential Methylation Hot Zones were identified as described earlier by calculating the p-value estimated from frequency of CG DMLs

(D1-MSN vs D2-MSN) in genome-wide 10 kb bins and then using Comp-p to aggregate the p-value significant bins.

## Chromosome conformation capture assay

### Hi-C library preparation

Hi-C library preparation was performed as previously reported with modifications<sup>88</sup>. FACS-sorted cells from NAc of individual mice were fixed in 2% formaldehyde (Fisher Scientific, #F79500, Waltham, MA, USA) with 3% BSA for 10 min at RT with rotation. Glycine (2 M) was then added to a final concentration of 0.25 M. Cells were incubated on ice for 15 min, washed once with 3% BSA in PBS and collected by centrifugation of 2500g for 5 min. Fixed cells were resuspended in 200  $\mu$ L lysis buffer (10 mM Tris-HCl, 10 mM NaCl, 0.2% IGEPAL CA-630, 1x protease inhibitor) and incubated on ice for 30 min. The nuclei were then pelleted and washed once with 1.4x NEB CutSmart buffer (NEB, #B6004, Ipswich, MA, USA), and resuspended in 200  $\mu$ L 1.4x NEB CutSmart buffer. Then the nuclei were permeabilized in 0.3% SDS with agitation for 30 min at 37 °C. Upon finishing of permeabilization, 50  $\mu$ L 10% Triton X-100 was added to the sample. Then, 10  $\mu$ L HindIII-HF (NEB, #R3104T, Ipswich, MA, USA) was added and the nuclei were digested at 37°C for 12 hours with 300 rpm agitation. Following digestion, a biotinylation mix (containing 4  $\mu$ L of 10x NEB cut smart buffer, 25  $\mu$ L of biotin-dATP (Invitrogen, #19524016, Carlsbad, CA, USA) 0.4 M, 6.4  $\mu$ L of DNA polymerase I large fragment 5000 U/mL, 1  $\mu$ L of 10 mM dCTP, dGTP and dTTP (NEB, #N0446S, Ipswich, MA, USA) mixture was added to the sample and incubated at 37 °C with agitation for an hour. Then, a ligation reaction was performed with ligation mix (containing 70  $\mu$ L of 10x T4 DNA ligase buffer (Invitrogen, #46300-018, Carlsbad, CA, USA), 3.5  $\mu$ L of 10% BSA, 15  $\mu$ L of T4 DNA ligase (Invitrogen, #15224-090, Carlsbad, CA, USA), 60  $\mu$ L of 10% Triton X-100) at 16 °C incubation for 4 hours followed by RT for 30 min. After ligation, nuclei were collected by centrifugation and reverse-crosslinking was then performed at 55 °C overnight with 15  $\mu$ L proteinase K. DNA was extracted using 0.4 x volume of SPRIselect beads and fragmented to an average size of 400 bp through a Covaris E220 sonicator. The DNA fragments were size-selected with a round of 0.6 x volume and another round of 0.9 x volume of SPRIselect beads, resuspended in 40  $\mu$ L TE and proceeded for biotin enrichment with Streptavidin MyOne T1 Dynabeads (Invitrogen, 65601, CA, USA) and library preparation with Accel-NGS 2S Plus DNA Library Kit (Swift, #21024, Ann Arbor, MI, USA). Firstly, 20  $\mu$ L of reaction mix with buffer/enzyme W1 -W2 was added to 40  $\mu$ L beads and incubated at 37 °C for 10 min. The beads underwent washing twice with NTB at 55 °C for 2 min and 1 time of washing with TE at RT. After each washing, beads were reclaimed by magnetic stand. The supernatant was removed after the TE washing, and the beads were resuspended in 50  $\mu$ L of reaction mix containing buffer/enzymes G1 - G4. After 20 min of incubation at 20 °C, the beads were washed twice with NTB buffer at 55 °C for 2 min, one wash with TE buffer at RT, and resuspended in 25  $\mu$ L of reaction buffer containing buffer/enzymes Y1 – Y3. This reaction mixture was incubated at 25 °C for 15 min and the beads were washed twice with NTB at 55 °C, once with TE at RT, resuspended in a 50  $\mu$ L reaction mixture containing buffer/enzymes B1 - B6, and incubated at 40 °C for 10 min. After twice washing with NTB at 55 °C, and once washing with TE at RT, the beads were resuspended in 25  $\mu$ L 10 mM elution buffer. The library was produced through eight cycles of PCR amplification with the resulting 25  $\mu$ L beads as templates. Finally, the Hi-C libraries were pooled and sequenced on the NovaSeq 6000 system with 100 bp pair-end runs.

## Hi-C data process

FASTQ files of Hi-C data were generated by the Illumina analysis pipeline. Adaptor trimming was performed on paired-end reads using Trim Galore 0.6.4 and Cutadapt 1.18. Low-quality sequences (Quality Phred score < 20) and reads shorter than 20 bp were removed. The processed reads were aligned to the mm10 mouse genome (for sequencing from male samples) or mm10 mouse genome without the Y chromosome (for sequencing from female samples) by Hi-C-Pro 2.11.4<sup>89</sup> with default setting for HindIII cutting sites. The alignment summary of Hi-C libraries is available in Table 9. The unique valid interaction pairs of each replicate were used to construct the Hi-C interaction matrix using “hicpro2juicebox.sh” of Hi-C-Pro and Juicer tools<sup>90</sup>, and visualization in Juicebox<sup>91</sup>.

## 3D genome organization analysis

The correlation between individual Hi-C replicates was assessed by stratum-adjusted correlation coefficients via HiCRep<sup>92</sup>. For the direct comparison of *Tet1* KO and Con Hi-C matrices, four groups of Hi-C matrices were normalized to an equal sequencing depth, with known genome gaps and duplicated regions (bad regions) masked, then compared using “hicCompareMatrices” of HiCExplorer<sup>93</sup>. To identify differentially interacting regions, the diagonal genomic interaction counts for each replicate in 1.5 Mb windows with 500k resolution were calculated by “bedtool map” of Bedtools, and then used for differential analysis of regional interactions in R with EdgeR<sup>94</sup>. The PC1 value of Hi-C compartments analysis was performed on sequencing depth-balanced matrices using hicPCA from HiCExplorer with previously published D1-MSN H3K4me3 ChIP-seq data (GSE197668) as a reference for D1-MSN active genomic regions<sup>38</sup>. The D1-MSN interaction peaks/loops were identified using HiCCUPs of Juicer tools at 5, 10, 25, and 50 kb resolutions with 0.1 FDR cutoff and merged at 25 kb resolution using “mergeBedpe” function of “hictools” (<https://github.com/EricSDavis/hictools>). Using these D1-MSN Hi-C loops as a reference, the loop scores of individual Hi-C replicates were calculated by “findTADsAndLoops.pl score” from HOMER at a resolution of 25 kb, which were then used for differentially interacting loop analyses by EdgeR. For visualization of Hi-C interactions, HiCExplorer<sup>95</sup> and pyGenomeTracks were applied. ATAC-seq data of striatum D1-MSN was retrieved (<http://catlas.org/mousebrain/#!/cellType>)<sup>96</sup> to visualize the chromatin accessibility in representative genes.

## **Annotation of DMR with Hi-C interaction loops and ranking TET1 target genes**

In addition to the annotation of DMR based on their proximity to genes, we conducted a second round of annotation integrating Hi-C loops. We annotated those DMRs located within Hi-C loop anchors as connected to the target gene at the opposite end of the loop interaction genomic regions. This allows us to explore the functional implication of DNA methylation change with genomic interaction informations. To visualize the epigenomic change of representative genes, IGV 2.12.3<sup>97</sup> was used to exhibit genomic tracks and mouse reference gene models.

To identify TET1-target genes implicated in drug addiction, we employed a ranking method for genes associated with D1-MSN CG DMR, DHZ, non-CG DML, Hi-C differentially interacting regions (DIRs), and differentially interacting loops (DILs). We then integrated these genes with two gene lists from previous studies: the NAc addiction index genes whose transcription level

correlating with mouse cocaine self-administration behaviors<sup>47</sup> and D1-MSN addiction-related genes identified based on D1-MSN cell-type specific regulatory elements profiling and genome-wide association studies<sup>46</sup>. Each association was assigned with equal weight, and genes were ranked by the cumulative score of all associations.

## Data availability

The raw and processed data generated from this study are available on NCBI Gene Expression Omnibus and Sequence Read Archive with accession number GSE256164 and GSE256165.

## Code availability

The code for the pipelines of WGBS and Hi-C data processes and related analysis is available at [https://github.com/juicybrain/D1-MSN\\_WGBS\\_Hi-C](https://github.com/juicybrain/D1-MSN_WGBS_Hi-C).

## Extended data files

**Extended Data Figure 1.** Sex specific roles of TET1 in cocaine extinction and cue-induced reinstatement of cocaine seeking.

**Extended Data Figure 2.** Sex specific roles of TET1 in sucrose self-administration, extinction and cue-induced reinstatement.

**Extended Data Figure 3.** Viral-mediated TET1 overexpression in mouse nucleus accumbens D1-medium spiny neurons.

**Extended Data Figure 4.** Nucleus accumbens D1 medium spiny neuron isolation and whole-genome DNA methylation profiling.

**Extended Data Figure 5.** Differentially methylation hot zones (DHZs) are characterized by high-frequency same direction of DNA methylation changes in a long genomic region.

**Extended Data Figure 6.** NAc MSN cell type-specific DHZs.

**Extended Data Figure 7.** Characterization of 3D genome interactions in D1-MSNs.

**Extended data Figure 8.** Integration of DNA methylation changes and Hi-C loops.

**Extended data Figure 9.** Identification of addiction associated D1-MSN TET1 target genes.

**Table 1:** Sequencing parameters of WGBS libraries

**Table 2:** D1-MSN CG DMRs

**Table 3:** CG DMGs gene ontology analysis

**Table 4:** Enriched transcription factor motifs in CG DMRs

**Table 5:** CG DMR clusters

**Table 6:** D1-MSN autosomal CG DMLs

**Table 7:** D1-MSN Differential Methylation Hot Zones (DHZs)

**Table 8: NAc MSN cell type-specific DHZs**

**Table 9: Summary of sequencing parameters of Hi-C libraries**

**Table 10: Hi-C differentially interacting bins**

**Table 11: D1-MSN Hi-C loops**

**Table 12: KEGG pathway analysis of sex-dimorphic DMGs**

**Table 13: GO analysis on D1-MSN DMRs with DHZ classification**

**Table 14: TET1-dependent differentially interacting loops**

**Table 15: Ranking of predicted TET1 target genes**

**Table 16: PCR primers used in this study**

Statistic files

## Acknowledgements

We thank Ruth Didier and Beth Alexander for the assistance in FACS. This work was supported by the National Institutes of Health (Grant Nos. DP1 DA046587 and R01 DA046720 [to J.F.]).

## Author contributions

H.X. performed animal raising, genotyping, FACS, mouse brain stereotaxic and jugular vein catheterization surgeries and behavioral experiments; H.X. and J.F. generated all the mutant mice; Y.L. performed genotyping, FACS, WGBS, Hi-C experiment, related bioinformatic analyses, and data visualization; Q.Y. and X.Z. performed electrophysiological recordings; N.J.W. helped on data processing at early time of this study; A.N.B., G.J.K. and C.E.R. performed animal raising and genotyping; J.M.C., K.A. and R.L.H. performed genotyping; J.M.C. and P.F. provided the technique support on Hi-C procedure; Y.L. and J.F. designed the virus; H.X., Y.L. performed data analyses. H.X., Y.L. X.Z. and J.F. wrote the manuscript; J.F. conceived the experiments and supervised the study.

## Competing Interests

The authors declare no competing interests.

## References

- 1 Cotto, J. H., Davis, E., Dowling, G. J., Elcano, J. C., Staton, A. B. & Weiss, S. R. Gender effects on drug use, abuse, and dependence: a special analysis of results from the National Survey on Drug Use and Health. *Gender medicine* **7**, 402-413, doi:10.1016/j.genm.2010.09.004 (2010).

- 2 Greenfield, S. F., Back, S. E., Lawson, K. & Brady, K. T. Substance abuse in women. *The Psychiatric clinics of North America* **33**, 339-355, doi:10.1016/j.psc.2010.01.004 (2010).
- 3 McHugh, R. K., Votaw, V. R., Sugarman, D. E. & Greenfield, S. F. Sex and gender differences in substance use disorders. *Clinical psychology review* **66**, 12-23, doi:10.1016/j.cpr.2017.10.012 (2018).
- 4 Becker, J. B. & Chartoff, E. Sex differences in neural mechanisms mediating reward and addiction. *Neuropsychopharmacology* **44**, 166-183, doi:10.1038/s41386-018-0125-6 (2019).
- 5 Ghahramani, N. M., Nguen, T. C., Chen, P. Y., Tian, Y., Krishnan, S., Muir, S., Rubbi, L., Arnold, A. P., de Vries, G. J., Forger, N. G., Pellegrini, M. & Vilain, E. The effects of perinatal testosterone exposure on the DNA methylome of the mouse brain are late-emerging. *Biol Sex Differ* **5**, 8, doi:10.1186/2042-6410-5-8 (2014).
- 6 Xia, Y., Dai, R., Wang, K., Jiao, C., Zhang, C., Xu, Y., Li, H., Jing, X., Chen, Y., Jiang, Y., Kopp, R. F., Giase, G., Chen, C. & Liu, C. Sex-differential DNA methylation and associated regulation networks in human brain implicated in the sex-biased risks of psychiatric disorders. *Mol Psychiatry* **26**, 835-848, doi:10.1038/s41380-019-0416-2 (2021).
- 7 Kolodkin, M. H. & Auger, A. P. Sex difference in the expression of DNA methyltransferase 3a in the rat amygdala during development. *Journal of neuroendocrinology* **23**, 577-583, doi:10.1111/j.1365-2826.2011.02147.x (2011).
- 8 Arnold, A. P. A general theory of sexual differentiation. *Journal of neuroscience research* **95**, 291-300, doi:10.1002/jnr.23884 (2017).
- 9 Nugent, B. M., Wright, C. L., Shetty, A. C., Hodes, G. E., Lenz, K. M., Mahurkar, A., Russo, S. J., Devine, S. E. & McCarthy, M. M. Brain feminization requires active repression of masculinization via DNA methylation. *Nat Neurosci* **18**, 690-697, doi:10.1038/nn.3988 (2015).
- 10 Feng, J. & Nestler, E. J. Epigenetic mechanisms of drug addiction. *Curr Opin Neurobiol* **23**, 521-528, doi:10.1016/j.conb.2013.01.001 (2013).
- 11 Hamilton, P. J. & Nestler, E. J. Epigenetics and addiction. *Curr Opin Neurobiol* **59**, 128-136, doi:10.1016/j.conb.2019.05.005 (2019).
- 12 Kaplan, G., Xu, H., Abreu, K. & Feng, J. DNA Epigenetics in Addiction Susceptibility. *Front Genet* **13**, 806685, doi:10.3389/fgene.2022.806685 (2022).
- 13 Ito, S., Shen, L., Dai, Q., Wu, S. C., Collins, L. B., Swenberg, J. A., He, C. & Zhang, Y. Tet proteins can convert 5-methylcytosine to 5-formylcytosine and 5-carboxylcytosine. *Science* **333**, 1300-1303, doi:10.1126/science.1210597 (2011).
- 14 Xu, G.-L. & Bochtler, M. Reversal of nucleobase methylation by dioxygenases. *Nature chemical biology* **16**, 1160-1169 (2020).
- 15 Wu, H. & Zhang, Y. Reversing DNA methylation: mechanisms, genomics, and biological functions. *Cell* **156**, 45-68, doi:10.1016/j.cell.2013.12.019 (2014).
- 16 Alaghband, Y., Bredy, T. W. & Wood, M. A. The role of active DNA demethylation and Tet enzyme function in memory formation and cocaine action. *Neuroscience letters* **625**, 40-46, doi:10.1016/j.neulet.2016.01.023 (2016).
- 17 Li, X., Wei, W., Ratnu, V. S. & Bredy, T. W. On the potential role of active DNA demethylation in establishing epigenetic states associated with neural plasticity and memory. *Neurobiology of learning and memory* **105**, 125-132, doi:10.1016/j.nlm.2013.06.009 (2013).
- 18 Rudenko, A., Dawlaty, M. M., Seo, J., Cheng, A. W., Meng, J., Le, T., Faull, K. F., Jaenisch, R. & Tsai, L. H. Tet1 is critical for neuronal activity-regulated gene expression and memory extinction. *Neuron* **79**, 1109-1122, doi:10.1016/j.neuron.2013.08.003 (2013).
- 19 Zhang, R. R., Cui, Q. Y., Murai, K., Lim, Y. C., Smith, Z. D., Jin, S., Ye, P., Rosa, L., Lee, Y. K., Wu, H. P., Liu, W., Xu, Z. M., Yang, L., Ding, Y. Q., Tang, F., Meissner, A., Ding, C., Shi, Y. & Xu, G. L. Tet1

- regulates adult hippocampal neurogenesis and cognition. *Cell Stem Cell* **13**, 237-245, doi:10.1016/j.stem.2013.05.006 (2013).
- 20 Anier, K., Urb, M., Kipper, K., Herodes, K., Timmusk, T., Zharkovsky, A. & Kalda, A. Cocaine-induced epigenetic DNA modification in mouse addiction-specific and non-specific tissues. *Neuropharmacology* **139**, 13-25, doi:10.1016/j.neuropharm.2018.06.036 (2018).
- 21 Jiang, F. Z., Zheng, W., Wu, C., Li, Y., Shen, F., Liang, J., Li, M., Zhang, J. J. & Sui, N. Double dissociation of inhibitory effects between the hippocampal TET1 and TET3 in the acquisition of morphine self-administration in rats. *Addiction biology* **26**, e12875, doi:10.1111/adb.12875 (2021).
- 22 Feng, J., Shao, N., Szulwach, K. E., Vialou, V., Huynh, J., Zhong, C., Le, T., Ferguson, D., Cahill, M. E., Li, Y., Koo, J. W., Ribeiro, E., Labonte, B., Laitman, B. M., Estey, D., Stockman, V., Kennedy, P., Courousse, T., Mensah, I., Turecki, G., Faull, K. F., Ming, G. L., Song, H., Fan, G., Casaccia, P., Shen, L., Jin, P. & Nestler, E. J. Role of Tet1 and 5-hydroxymethylcytosine in cocaine action. *Nat Neurosci* **18**, 536-544, doi:10.1038/nn.3976 (2015).
- 23 Gerfen, C. R. & Surmeier, D. J. Modulation of striatal projection systems by dopamine. *Annu Rev Neurosci* **34**, 441-466, doi:10.1146/annurev-neuro-061010-113641 (2011).
- 24 Lobo, M. K. & Nestler, E. J. The striatal balancing act in drug addiction: distinct roles of direct and indirect pathway medium spiny neurons. *Front Neuroanat* **5**, 41, doi:10.3389/fnana.2011.00041 (2011).
- 25 Bock, R., Shin, J. H., Kaplan, A. R., Dobi, A., Markey, E., Kramer, P. F., Gremel, C. M., Christensen, C. H., Adrover, M. F. & Alvarez, V. A. Strengthening the accumbal indirect pathway promotes resilience to compulsive cocaine use. *Nat Neurosci* **16**, 632-638, doi:10.1038/nn.3369 (2013).
- 26 Pardo-Garcia, T. R., Garcia-Keller, C., Penalosa, T., Richie, C. T., Pickel, J., Hope, B. T., Harvey, B. K., Kalivas, P. W. & Heinsbroek, J. A. Ventral Pallidum Is the Primary Target for Accumbens D1 Projections Driving Cocaine Seeking. *J Neurosci* **39**, 2041-2051, doi:10.1523/JNEUROSCI.2822-18.2018 (2019).
- 27 Saad, L., Sartori, M., Pol Bodetto, S., Romieu, P., Kalsbeek, A., Zwiller, J. & Anglard, P. Regulation of Brain DNA Methylation Factors and of the Orexinergic System by Cocaine and Food Self-Administration. *Molecular neurobiology* **56**, 5315-5331, doi:10.1007/s12035-018-1453-6 (2019).
- 28 Guo, J. U., Su, Y., Zhong, C., Ming, G. L. & Song, H. Hydroxylation of 5-methylcytosine by TET1 promotes active DNA demethylation in the adult brain. *Cell* **145**, 423-434, doi:10.1016/j.cell.2011.03.022 (2011).
- 29 Kaas, G. A., Zhong, C., Eason, D. E., Ross, D. L., Vachhani, R. V., Ming, G. L., King, J. R., Song, H. & Sweatt, J. D. TET1 controls CNS 5-methylcytosine hydroxylation, active DNA demethylation, gene transcription, and memory formation. *Neuron* **79**, 1086-1093, doi:10.1016/j.neuron.2013.08.032 (2013).
- 30 Wu, X. & Zhang, Y. TET-mediated active DNA demethylation: mechanism, function and beyond. *Nat Rev Genet* **18**, 517-534, doi:10.1038/nrg.2017.33 (2017).
- 31 Li, Y., Xu, H., Chitaman, J. M. & Feng, J. Whole Genome DNA Methylation Profiling of D2 Medium Spiny Neurons in Mouse Nucleus Accumbens Using Two Independent Library Preparation Methods. *Genes (Basel)* **13**, doi:10.3390/genes13020306 (2022).
- 32 Spruijt, C. G., Gnerlich, F., Smits, A. H., Pfaffeneder, T., Jansen, P. W., Bauer, C., Munzel, M., Wagner, M., Muller, M., Khan, F., Eberl, H. C., Mensinga, A., Brinkman, A. B., Lepikhov, K., Muller, U., Walter, J., Boelens, R., van Ingen, H., Leonhardt, H., Carell, T. & Vermeulen, M. Dynamic readers for 5-(hydroxy)methylcytosine and its oxidized derivatives. *Cell* **152**, 1146-1159, doi:10.1016/j.cell.2013.02.004 (2013).
- 33 Tate, P. H. & Bird, A. P. Effects of DNA methylation on DNA-binding proteins and gene expression. *Curr Opin Genet Dev* **3**, 226-231, doi:10.1016/0959-437X(93)90027-m (1993).

- 34 Pulipparacharuvil, S., Renthal, W., Hale, C. F., Taniguchi, M., Xiao, G., Kumar, A., Russo, S. J., Sikder, D., Dewey, C. M., Davis, M. M., Greengard, P., Nairn, A. C., Nestler, E. J. & Cowan, C. W. Cocaine regulates MEF2 to control synaptic and behavioral plasticity. *Neuron* **59**, 621-633, doi:10.1016/j.neuron.2008.06.020 (2008).
- 35 Malik, A. N., Vierbuchen, T., Hemberg, M., Rubin, A. A., Ling, E., Couch, C. H., Stroud, H., Spiegel, I., Farh, K. K., Harmin, D. A. & Greenberg, M. E. Genome-wide identification and characterization of functional neuronal activity-dependent enhancers. *Nat Neurosci* **17**, 1330-1339, doi:10.1038/nn.3808 (2014).
- 36 Flavell, S. W. & Greenberg, M. E. Signaling mechanisms linking neuronal activity to gene expression and plasticity of the nervous system. *Annu Rev Neurosci* **31**, 563-590, doi:10.1146/annurev.neuro.31.060407.125631 (2008).
- 37 Teague, C. D. & Nestler, E. J. Key transcription factors mediating cocaine-induced plasticity in the nucleus accumbens. *Mol Psychiatry* **27**, 687-709, doi:10.1038/s41380-021-01163-5 (2022).
- 38 Yeh, S. Y., Estill, M., Lardner, C. K., Browne, C. J., Minier-Toribio, A., Futamura, R., Beach, K., McManus, C. A., Xu, S. J., Zhang, S., Heller, E. A., Shen, L. & Nestler, E. J. Cell Type-Specific Whole-Genome Landscape of DeltaFOSB Binding in the Nucleus Accumbens After Chronic Cocaine Exposure. *Biol Psychiatry* **94**, 367-377, doi:10.1016/j.biopsych.2022.12.021 (2023).
- 39 Bolzer A, K. G., Solovei I, Koehler D, Saracoglu K, Fauth C, et al. Three-Dimensional Maps of All Chromosomes in Human Male Fibroblast Nuclei and Prometaphase Rosettes. *PLoS Biology PLoS Biol* **3(5)**: e157, doi:doi.org/10.1371/journal.pbio.0030157 (2005).
- 40 Bonev, B. & Cavalli, G. Organization and function of the 3D genome. *Nat Rev Genet* **17**, 772, doi:10.1038/nrg.2016.147 (2016).
- 41 Carter, D., Chakalova, L., Osborne, C. S., Dai, Y. F. & Fraser, P. Long-range chromatin regulatory interactions in vivo. *Nat Genet* **32**, 623-626, doi:10.1038/ng1051 (2002).
- 42 Lieberman-Aiden, E., van Berkum, N. L., Williams, L., Imakaev, M., Ragoczy, T., Telling, A., Amit, I., Lajoie, B. R., Sabo, P. J., Dorschner, M. O., Sandstrom, R., Bernstein, B., Bender, M. A., Groudine, M., Gnirke, A., Stamatoyannopoulos, J., Mirny, L. A., Lander, E. S. & Dekker, J. Comprehensive mapping of long-range interactions reveals folding principles of the human genome. *Science* **326**, 289-293, doi:10.1126/science.1181369 (2009).
- 43 Nagano, T., Lubling, Y., Stevens, T. J., Schoenfelder, S., Yaffe, E., Dean, W., Laue, E. D., Tanay, A. & Fraser, P. Single-cell Hi-C reveals cell-to-cell variability in chromosome structure. *Nature* **502**, 59-64, doi:10.1038/nature12593 (2013).
- 44 Suhas S.P. Rao, M. H. H., Neva C. Durand, Elena K. Stamenova, Ivan D. Bochkov, James T. Robinson, Adrian L. Sanborn, Ido Machol, Arina D. Omer, Eric S. Lander, Erez Lieberman Aiden. A 3D Map of the Human Genome at Kilobase Resolution Reveals Principles of Chromatin Looping. *Cell* **159**, 1665-1680, doi:doi.org/10.1016/j.cell.2014.11.021 (2015).
- 45 Zhou, X., Li, A., Mi, X., Li, Y., Ding, Z., An, M., Chen, Y., Li, W., Tao, X., Chen, X. & Li, Y. Hyperexcited limbic neurons represent sexual satiety and reduce mating motivation. *Science* **379**, 820-825, doi:10.1126/science.abl4038 (2023).
- 46 Srinivasan, C., Phan, B. N., Lawler, A. J., Ramamurthy, E., Kleymen, M., Brown, A. R., Kaplow, I. M., Wirthlin, M. E. & Pfenning, A. R. Addiction-Associated Genetic Variants Implicate Brain Cell Type- and Region-Specific Cis-Regulatory Elements in Addiction Neurobiology. *J Neurosci* **41**, 9008-9030, doi:10.1523/JNEUROSCI.2534-20.2021 (2021).
- 47 Walker, D. M., Cates, H. M., Loh, Y. E., Purushothaman, I., Ramakrishnan, A., Cahill, K. M., Lardner, C. K., Godino, A., Kronman, H. G., Rabkin, J., Lorsch, Z. S., Mews, P., Doyle, M. A., Feng, J., Labonte, B., Koo, J. W., Bagot, R. C., Logan, R. W., Seney, M. L., Calipari, E. S., Shen, L. & Nestler, E. J. Cocaine Self-administration Alters Transcriptome-wide Responses in the Brain's Reward Circuitry. *Biol Psychiatry* **84**, 867-880, doi:10.1016/j.biopsych.2018.04.009 (2018).

- 48 Engmann, O., Labonte, B., Mitchell, A., Bashtrykov, P., Calipari, E. S., Rosenbluh, C., Loh, Y. H. E., Walker, D. M., Burek, D., Hamilton, P. J., Issler, O., Neve, R. L., Turecki, G., Hurd, Y., Chess, A., Shen, L., Mansuy, I., Jeltsch, A., Akbarian, S. & Nestler, E. J. Cocaine-Induced Chromatin Modifications Associate With Increased Expression and Three-Dimensional Looping of AutS2. *Biological Psychiatry* **82**, 794-805 (2017).
- 49 Vian, L., Pekowska, A., Rao, S. S. P., Kieffer-Kwon, K. R., Jung, S., Baranello, L., Huang, S. C., El Khattabi, L., Dose, M., Pruett, N., Sanborn, A. L., Canela, A., Maman, Y., Oksanen, A., Resch, W., Li, X., Lee, B., Kovalchuk, A. L., Tang, Z., Nelson, S., Di Pierro, M., Cheng, R. R., Machol, I., St Hilaire, B. G., Durand, N. C., Shamim, M. S., Stamenova, E. K., Onuchic, J. N., Ruan, Y., Nussenzweig, A., Levens, D., Aiden, E. L. & Casellas, R. The Energetics and Physiological Impact of Cohesin Extrusion. *Cell* **173**, 1165-1178 e1120, doi:10.1016/j.cell.2018.03.072 (2018).
- 50 Hu, M., Crombag, H. S., Robinson, T. E. & Becker, J. B. Biological basis of sex differences in the propensity to self-administer cocaine. *Neuropsychopharmacology* **29**, 81-85, doi:10.1038/sj.npp.1300301 (2004).
- 51 Jackson, L. R., Robinson, T. E. & Becker, J. B. Sex differences and hormonal influences on acquisition of cocaine self-administration in rats. *Neuropsychopharmacology* **31**, 129-138, doi:10.1038/sj.npp.1300778 (2006).
- 52 Lynch, W. J. & Carroll, M. E. Sex differences in the acquisition of intravenously self-administered cocaine and heroin in rats. *Psychopharmacology* **144**, 77-82, doi:10.1007/s002130050979 (1999).
- 53 Lopez, A. J., Johnson, A. R., Euston, T. J., Wilson, R., Nolan, S. O., Brady, L. J., Thibeault, K. C., Kelly, S. J., Kondev, V., Melugin, P., Kutlu, M. G., Chuang, E., Lam, T. T., Kiraly, D. D. & Calipari, E. S. Cocaine self-administration induces sex-dependent protein expression in the nucleus accumbens. *Commun Biol* **4**, 883, doi:10.1038/s42003-021-02358-w (2021).
- 54 Feng, J., Pena, C. J., Purushothaman, I., Engmann, O., Walker, D., Brown, A. N., Issler, O., Doyle, M., Harrigan, E., Mouzon, E., Vialou, V., Shen, L., Dawlaty, M. M., Jaenisch, R. & Nestler, E. J. Tet1 in Nucleus Accumbens Opposes Depression- and Anxiety-Like Behaviors. *Neuropsychopharmacology* **42**, 1657-1669, doi:10.1038/npp.2017.6 (2017).
- 55 Becker, J. B. & Koob, G. F. Sex Differences in Animal Models: Focus on Addiction. *Pharmacological reviews* **68**, 242-263, doi:10.1124/pr.115.011163 (2016).
- 56 Lopez-Moyado, I. F., Tsagarakis, A., Yuita, H., Seo, H., Delatte, B., Heinz, S., Benner, C. & Rao, A. Paradoxical association of TET loss of function with genome-wide DNA hypomethylation. *Proc Natl Acad Sci U S A* **116**, 16933-16942, doi:10.1073/pnas.1903059116 (2019).
- 57 Liu, H., Zhou, J., Tian, W., Luo, C., Bartlett, A., Aldridge, A., Lucero, J., Osteen, J. K., Nery, J. R., Chen, H., Rivkin, A., Castanon, R. G., Clock, B., Li, Y. E., Hou, X., Poirion, O. B., Preissl, S., Pinto-Duarte, A., O'Connor, C., Boggeman, L., Fitzpatrick, C., Nunn, M., Mukamel, E. A., Zhang, Z., Callaway, E. M., Ren, B., Dixon, J. R., Behrens, M. M. & Ecker, J. R. DNA methylation atlas of the mouse brain at single-cell resolution. *Nature* **598**, 120-128, doi:10.1038/s41586-020-03182-8 (2021).
- 58 Rizzardi, L. F., Hickey, P. F., Rodriguez DiBlasi, V., Tryggvadottir, R., Callahan, C. M., Idrizi, A., Hansen, K. D. & Feinberg, A. P. Neuronal brain-region-specific DNA methylation and chromatin accessibility are associated with neuropsychiatric trait heritability. *Nat Neurosci* **22**, 307-316, doi:10.1038/s41593-018-0297-8 (2019).
- 59 Tian, W., Zhou, J., Bartlett, A., Zeng, Q., Liu, H., Castanon, R. G., Kenworthy, M., Altshul, J., Valadon, C., Aldridge, A., Nery, J. R., Chen, H., Xu, J., Johnson, N. D., Lucero, J., Osteen, J. K., Emerson, N., Rink, J., Lee, J., Li, Y. E., Siletti, K., Liem, M., Claffey, N., O'Connor, C., Yanny, A. M., Nyhus, J., Dee, N., Casper, T., Shapovalova, N., Hirschstein, D., Ding, S. L., Hodge, R., Levi, B. P., Keene, C. D., Linnarsson, S., Lein, E., Ren, B., Behrens, M. M. & Ecker, J. R. Single-cell DNA methylation and 3D genome architecture in the human brain. *Science* **382**, eadf5357, doi:10.1126/science.adf5357 (2023).

- 60 Dileep, V., Boix, C. A., Mathys, H., Marco, A., Welch, G. M., Meharena, H. S., Loon, A., Jeloka, R., Peng, Z., Bennett, D. A., Kellis, M. & Tsai, L. H. Neuronal DNA double-strand breaks lead to genome structural variations and 3D genome disruption in neurodegeneration. *Cell* **186**, 4404-4421 e4420, doi:10.1016/j.cell.2023.08.038 (2023).
- 61 Zhang, W., Xia, W., Wang, Q., Towers, A. J., Chen, J., Gao, R., Zhang, Y., Yen, C. A., Lee, A. Y., Li, Y., Zhou, C., Liu, K., Zhang, J., Gu, T. P., Chen, X., Chang, Z., Leung, D., Gao, S., Jiang, Y. H. & Xie, W. Isoform Switch of TET1 Regulates DNA Demethylation and Mouse Development. *Mol Cell* **64**, 1062-1073, doi:10.1016/j.molcel.2016.10.030 (2016).
- 62 Buitrago, D., Labrador, M., Arcon, J. P., Lema, R., Flores, O., Esteve-Codina, A., Blanc, J., Villegas, N., Bellido, D., Gut, M., Dans, P. D., Heath, S. C., Gut, I. G., Brun Heath, I. & Orozco, M. Impact of DNA methylation on 3D genome structure. *Nat Commun* **12**, 3243, doi:10.1038/s41467-021-23142-8 (2021).
- 63 Xu, J., Song, F., Lyu, H., Kobayashi, M., Zhang, B., Zhao, Z., Hou, Y., Wang, X., Luan, Y., Jia, B., Stasiak, L., Wong, J. H., Wang, Q., Jin, Q., Jin, Q., Fu, Y., Yang, H., Hardison, R. C., Dovat, S., Plataniolas, L. C., Diao, Y., Yang, Y., Yamada, T., Viny, A. D., Levine, R. L., Claxton, D., Broach, J. R., Zheng, H. & Yue, F. Subtype-specific 3D genome alteration in acute myeloid leukaemia. *Nature* **611**, 387-398, doi:10.1038/s41586-022-05365-x (2022).
- 64 Cao, J., Dorris, D. M. & Meitzen, J. Electrophysiological properties of medium spiny neurons in the nucleus accumbens core of prepubertal male and female Drd1a-tdTomato line 6 BAC transgenic mice. *J Neurophysiol* **120**, 1712-1727, doi:10.1152/jn.00257.2018 (2018).
- 65 Meadows, J. P., Guzman-Karlsson, M. C., Phillips, S., Holleman, C., Posey, J. L., Day, J. J., Hablitz, J. J. & Sweatt, J. D. DNA methylation regulates neuronal glutamatergic synaptic scaling. *Sci Signal* **8**, ra61, doi:10.1126/scisignal.aab0715 (2015).
- 66 Benarroch, E. E. HCN channels: function and clinical implications. *Neurology* **80**, 304-310, doi:10.1212/WNL.0b013e31827dec42 (2013).
- 67 McCarthy, M. M., Nugent, B. M. & Lenz, K. M. Neuroimmunology and neuroepigenetics in the establishment of sex differences in the brain. *Nature reviews. Neuroscience* **18**, 471-484, doi:10.1038/nrn.2017.61 (2017).
- 68 Becker, J. B., Arnold, A. P., Berkley, K. J., Blaustein, J. D., Eckel, L. A., Hampson, E., Herman, J. P., Marts, S., Sadee, W., Steiner, M., Taylor, J. & Young, E. Strategies and methods for research on sex differences in brain and behavior. *Endocrinology* **146**, 1650-1673, doi:10.1210/en.2004-1142 (2005).
- 69 Clayton, J. A. & Collins, F. S. Policy: NIH to balance sex in cell and animal studies. *Nature* **509**, 282-283, doi:10.1038/509282a (2014).
- 70 Dawlaty, M. M., Ganz, K., Powell, B. E., Hu, Y. C., Markoulaki, S., Cheng, A. W., Gao, Q., Kim, J., Choi, S. W., Page, D. C. & Jaenisch, R. Tet1 is dispensable for maintaining pluripotency and its loss is compatible with embryonic and postnatal development. *Cell Stem Cell* **9**, 166-175, doi:10.1016/j.stem.2011.07.010 (2011).
- 71 Zhao, Z., Chen, L., Dawlaty, M. M., Pan, F., Weeks, O., Zhou, Y., Cao, Z., Shi, H., Wang, J., Lin, L., Chen, S., Yuan, W., Qin, Z., Ni, H., Nimer, S. D., Yang, F. C., Jaenisch, R., Jin, P. & Xu, M. Combined Loss of Tet1 and Tet2 Promotes B Cell, but Not Myeloid Malignancies, in Mice. *Cell Rep* **13**, 1692-1704, doi:10.1016/j.celrep.2015.10.037 (2015).
- 72 Gong, S., Doughty, M., Harbaugh, C. R., Cummins, A., Hatten, M. E., Heintz, N. & Gerfen, C. R. Targeting Cre recombinase to specific neuron populations with bacterial artificial chromosome constructs. *J Neurosci* **27**, 9817-9823, doi:10.1523/JNEUROSCI.2707-07.2007 (2007).
- 73 Shuen, J. A., Chen, M., Gloss, B. & Calakos, N. Drd1a-tdTomato BAC transgenic mice for simultaneous visualization of medium spiny neurons in the direct and indirect pathways of the basal ganglia. *J Neurosci* **28**, 2681-2685, doi:10.1523/JNEUROSCI.5492-07.2008 (2008).

- 74 Xu, H., Brown, A. N., Waddell, N. J., Liu, X., Kaplan, G. J., Chitaman, J. M., Stockman, V., Hedinger, R. L., Adams, R., Abreu, K., Shen, L., Neve, R., Wang, Z., Nestler, E. J. & Feng, J. Role of Long Noncoding RNA Gas5 in Cocaine Action. *Biol Psychiatry* **88**, 758-766, doi:10.1016/j.biopsych.2020.05.004 (2020).
- 75 Martin, M. Cutadapt removes adapter sequences from high-throughput sequencing reads. *EMBnet. journal* **17**, 10-12 (2011).
- 76 Krueger, F. & Andrews, S. R. Bismark: a flexible aligner and methylation caller for Bisulfite-Seq applications. *bioinformatics* **27**, 1571-1572 (2011).
- 77 Langmead, B. & Salzberg, S. L. Fast gapped-read alignment with Bowtie 2. *Nature Methods* **9**, 357-U354, doi:10.1038/Nmeth.1923 (2012).
- 78 Ramirez, F., Ryan, D. P., Gruning, B., Bhardwaj, V., Kilpert, F., Richter, A. S., Heyne, S., Dundar, F. & Manke, T. deepTools2: a next generation web server for deep-sequencing data analysis. *Nucleic Acids Res* **44**, W160-165, doi:10.1093/nar/gkw257 (2016).
- 79 Quinlan, A. R. & Hall, I. M. BEDTools: a flexible suite of utilities for comparing genomic features. *Bioinformatics* **26**, 841-842, doi:10.1093/bioinformatics/btq033 (2010).
- 80 Feng, H., Conneely, K. N. & Wu, H. A Bayesian hierarchical model to detect differentially methylated loci from single nucleotide resolution sequencing data. *Nucleic Acids Research* **42**, doi:10.1093/nar/gku154 (2014).
- 81 Hansen, K. D., Langmead, B. & Irizarry, R. A. BSmooth: from whole genome bisulfite sequencing reads to differentially methylated regions. *Genome Biol* **13**, R83, doi:10.1186/gb-2012-13-10-r83 (2012).
- 82 Yu, G., Wang, L. G. & He, Q. Y. ChIPseeker: an R/Bioconductor package for ChIP peak annotation, comparison and visualization. *Bioinformatics* **31**, 2382-2383, doi:10.1093/bioinformatics/btv145 (2015).
- 83 Yu, G., Wang, L. G., Han, Y. & He, Q. Y. clusterProfiler: an R package for comparing biological themes among gene clusters. *Omics* **16**, 284-287, doi:10.1089/omi.2011.0118 (2012).
- 84 Heinz, S., Benner, C., Spann, N., Bertolino, E., Lin, Y. C., Laslo, P., Cheng, J. X., Murre, C., Singh, H. & Glass, C. K. Simple combinations of lineage-determining transcription factors prime cis-regulatory elements required for macrophage and B cell identities. *Mol Cell* **38**, 576-589, doi:10.1016/j.molcel.2010.05.004 (2010).
- 85 Gu, Z., Eils, R. & Schlesner, M. Complex heatmaps reveal patterns and correlations in multidimensional genomic data. *Bioinformatics* **32**, 2847-2849, doi:10.1093/bioinformatics/btw313 (2016).
- 86 Pedersen, B. S., Schwartz, D. A., Yang, I. V. & Kechris, K. J. Comb-p: software for combining, analyzing, grouping and correcting spatially correlated P-values. *Bioinformatics* **28**, 2986-2988, doi:10.1093/bioinformatics/bts545 (2012).
- 87 Lister, R., Mukamel, E. A., Nery, J. R., Urich, M., Puddifoot, C. A., Johnson, N. D., Lucero, J., Huang, Y., Dwork, A. J., Schultz, M. D., Yu, M., Toni-Tilippini, J., Heyn, H., Hu, S. J., Wu, J. C., Rao, A., Esteller, M., He, C., Haghghi, F. G., Sejnowski, T. J., Behrens, M. M. & Ecker, J. R. Global Epigenomic Reconfiguration During Mammalian Brain Development. *Science* **341**, doi:10.1126/science.1237905 (2013).
- 88 Schoenfelder, S., Javierre, B. M., Furlan-Magaril, M., Wingett, S. W. & Fraser, P. Promoter Capture Hi-C: High-resolution, Genome-wide Profiling of Promoter Interactions. *J Vis Exp*, doi:10.3791/57320 (2018).
- 89 Servant, N., Varoquaux, N., Lajoie, B. R., Viara, E., Chen, C. J., Vert, J. P., Heard, E., Dekker, J. & Barillot, E. HiC-Pro: an optimized and flexible pipeline for Hi-C data processing. *Genome Biol* **16**, 259, doi:10.1186/s13059-015-0831-x (2015).

- 90 Durand, N. C., Shamim, M. S., Machol, I., Rao, S. S., Huntley, M. H., Lander, E. S. & Aiden, E. L. Juicer Provides a One-Click System for Analyzing Loop-Resolution Hi-C Experiments. *Cell Syst* **3**, 95-98, doi:10.1016/j.cels.2016.07.002 (2016).
- 91 Durand, N. C., Robinson, J. T., Shamim, M. S., Machol, I., Mesirov, J. P., Lander, E. S. & Aiden, E. L. Juicebox Provides a Visualization System for Hi-C Contact Maps with Unlimited Zoom. *Cell Syst* **3**, 99-101, doi:10.1016/j.cels.2015.07.012 (2016).
- 92 Yang, T., Zhang, F., Yardimci, G. G., Song, F., Hardison, R. C., Noble, W. S., Yue, F. & Li, Q. HiCRep: assessing the reproducibility of Hi-C data using a stratum-adjusted correlation coefficient. *Genome Res* **27**, 1939-1949, doi:10.1101/gr.220640.117 (2017).
- 93 Lopez-Delisle, L., Rabbani, L., Wolff, J., Bhardwaj, V., Backofen, R., Gruning, B., Ramirez, F. & Manke, T. pyGenomeTracks: reproducible plots for multivariate genomic datasets. *Bioinformatics* **37**, 422-423, doi:10.1093/bioinformatics/btaa692 (2021).
- 94 Robinson, M. D., McCarthy, D. J. & Smyth, G. K. edgeR: a Bioconductor package for differential expression analysis of digital gene expression data. *Bioinformatics* **26**, 139-140, doi:10.1093/bioinformatics/btp616 (2010).
- 95 Wolff, J., Bhardwaj, V., Nothjunge, S., Richard, G., Renschler, G., Gilsbach, R., Manke, T., Backofen, R., Ramirez, F. & Gruning, B. A. Galaxy HiCExplorer: a web server for reproducible Hi-C data analysis, quality control and visualization. *Nucleic Acids Res* **46**, W11-W16, doi:10.1093/nar/gky504 (2018).
- 96 Li, Y. E., Preissl, S., Hou, X., Zhang, Z., Zhang, K., Qiu, Y., Poirion, O. B., Li, B., Chiou, J., Liu, H., Pinto-Duarte, A., Kubo, N., Yang, X., Fang, R., Wang, X., Han, J. Y., Lucero, J., Yan, Y., Miller, M., Kuan, S., Gorkin, D., Gaulton, K. J., Shen, Y., Nunn, M., Mukamel, E. A., Behrens, M. M., Ecker, J. R. & Ren, B. An atlas of gene regulatory elements in adult mouse cerebrum. *Nature* **598**, 129-136, doi:10.1038/s41586-021-03604-1 (2021).
- 97 Thorvaldsdottir, H., Robinson, J. T. & Mesirov, J. P. Integrative Genomics Viewer (IGV): high-performance genomics data visualization and exploration. *Brief Bioinform* **14**, 178-192, doi:10.1093/bib/bbs017 (2013).

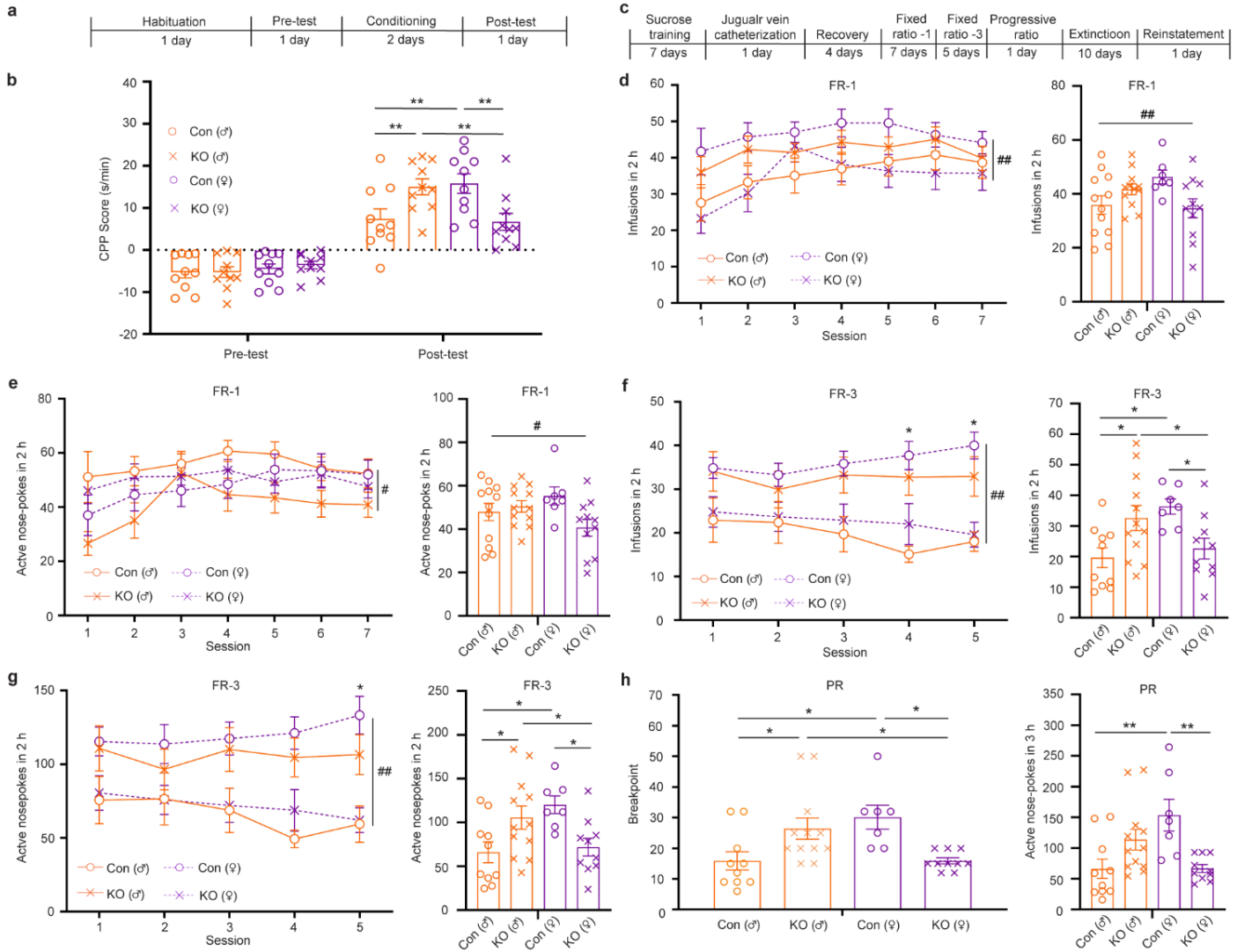


**Figure 1. Sex-specific role of TET1 in mediating cocaine addiction-like behaviors in D1-medium spiny neurons.** (a) Schematic diagram of the timeline of cocaine conditioned place preference (CPP) procedure. One day after habituation, a baseline pre-test was performed. Mice were then grouped for cocaine conditioning in two consecutive days, after which a post-test was carried out. (b) Cocaine CPP of control (Con) and *Tet1* knockout (KO) mice of both sexes. sex × genotype (F1, 136 = 9.415, p = 0.0041), \*\* p < 0.01. (c) Schematic diagram of the timeline of cocaine intravenous self-administration. All mice underwent sucrose training before a jugular vein catheterization surgery when a dwelling catheter was implanted. Mice were then trained to self-administer cocaine under schedules of fixed ratio-1 (FR-1), FR-3 and progressive ratio (PR), in order, with one session per day. Extinction and cue-induced reinstatement of cocaine seeking were characterized afterwards (data shown in Extended Data Fig. 1). (d) Number of cocaine infusions under FR-1 schedule. Left, daily average number of cocaine infusions across the seven-day schedule. Right, seven-day average number of cocaine infusions in each group. #: sex × genotype (F1, 38 = 7.852, p = 0.0079). (e) Number of active nose-pokes under FR-1, with daily average (left) and seven-day average (right) shown. #: sex × genotype (F1, 38 = 5.174, p = 0.0287). (f) Number of cocaine infusions under FR-3, with daily average (left) and five-day average (right) shown. Left, #: sex × genotype (F1, 35 = 14.40, p = 0.0012); \* p < 0.05 con (♀) vs con (♂). Right, \* #: sex × genotype (F1, 35 = 16.29, p = 0.0003). (g) Number of active nose-pokes under FR-3, with daily average (left) and five-day average (right) shown. Left, #: sex × genotype (F1, 35 = 12.11, p = 0.0014); \* #: sex × genotype (F1, 35 = 16.29, p = 0.0003). (h) Breakpoints and active nose-pokes under PR schedule. Left: breakpoint. sex × genotype (F1, 35 = 16.29, p = 0.0003), \* p < 0.05. Right: active number of active nose-pokes under PR schedule. \*\* p < 0.01. In cocaine CPP, n = 10 in each group. In cocaine self-administration, n = 7 - 12 in each group. Data are presented as mean ± SEM.

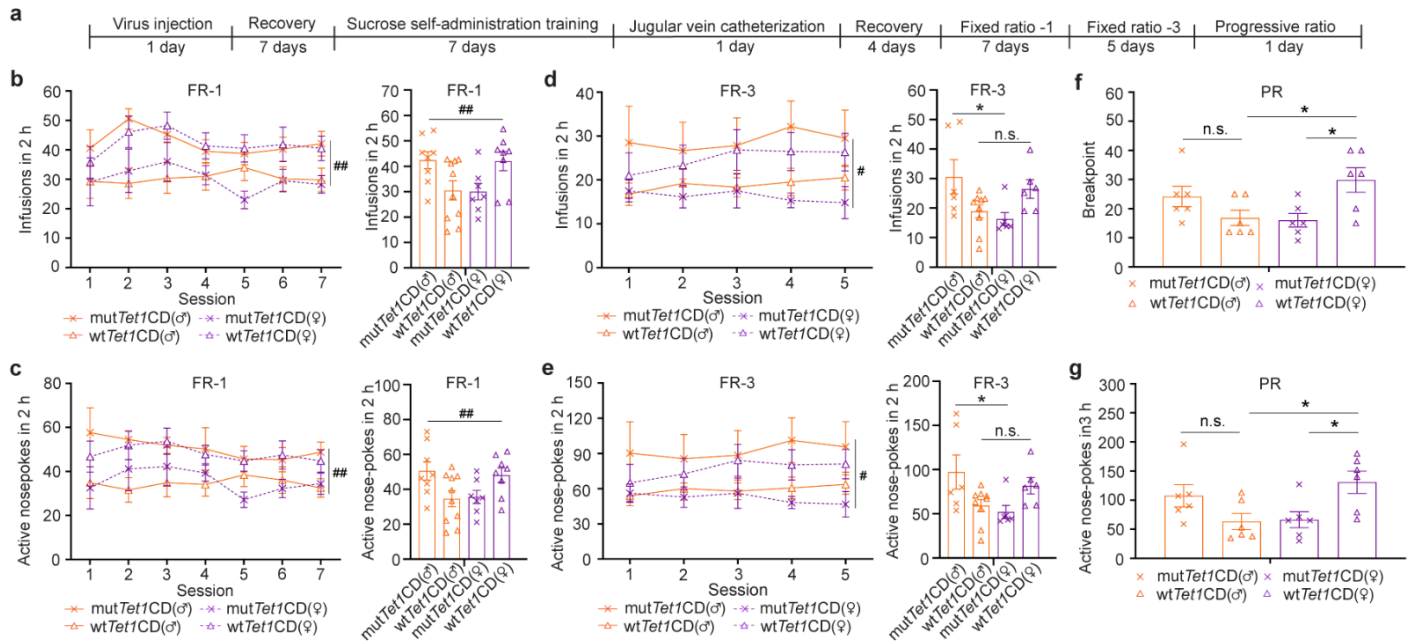


**Figure 2. Cocaine self-administration after viral mediated TET1 restoration in D1-Tet1 KO MSNs in nucleus accumbens.**

(a) Schematic diagram of experimental procedure. D1-Cre Tet1 KO mice received cre dependent Flex-on AAV-mutantTet1CD (mutTet1CD) or AAV-wildtypeTet1CD (wtTet1CD) injection in nucleus accumbens (NAc). After recovering, all mice were subjected to cocaine self-administration procedure similarly done as in Fig. 1c. (b) Number of cocaine infusions under FR-1 schedule. Left, daily average number of cocaine infusions across the seven-day period of FR-1. Right, seven-day average number of cocaine infusions in each group. ##: sex × virus (F1, 28 = 11.89, p = 0.0018). (c) Number of active nose pokes under FR-1, with daily average (left) and seven-day average (right) shown. ##: sex × virus (F1, 28 = 11.34, p = 0.0022). (d) Number of cocaine infusions under FR-3, with daily average (left) and five-day average (right) shown. #: sex × virus (F1, 23 = 5.695, p = 0.0256). \* p < 0.05. (e) Number of active nose-pokes under FR-3, with daily average (left) and five-day average (right) shown. #: sex × virus (F1, 23 = 5.423, p = 0.0290). \* p < 0.05. (f) Breakpoints earned under progressive ratio (PR) schedule. sex × virus (F1, 20 = 10.55, p = 0.0040). \* p < 0.05. (g) Number of active nose-pokes under PR. sex × virus (F1, 20 = 10.51, p = 0.0041). \* p < 0.05. n = 6 - 9 in each group. Data are presented as mean ± SEM. n.s., no significance.

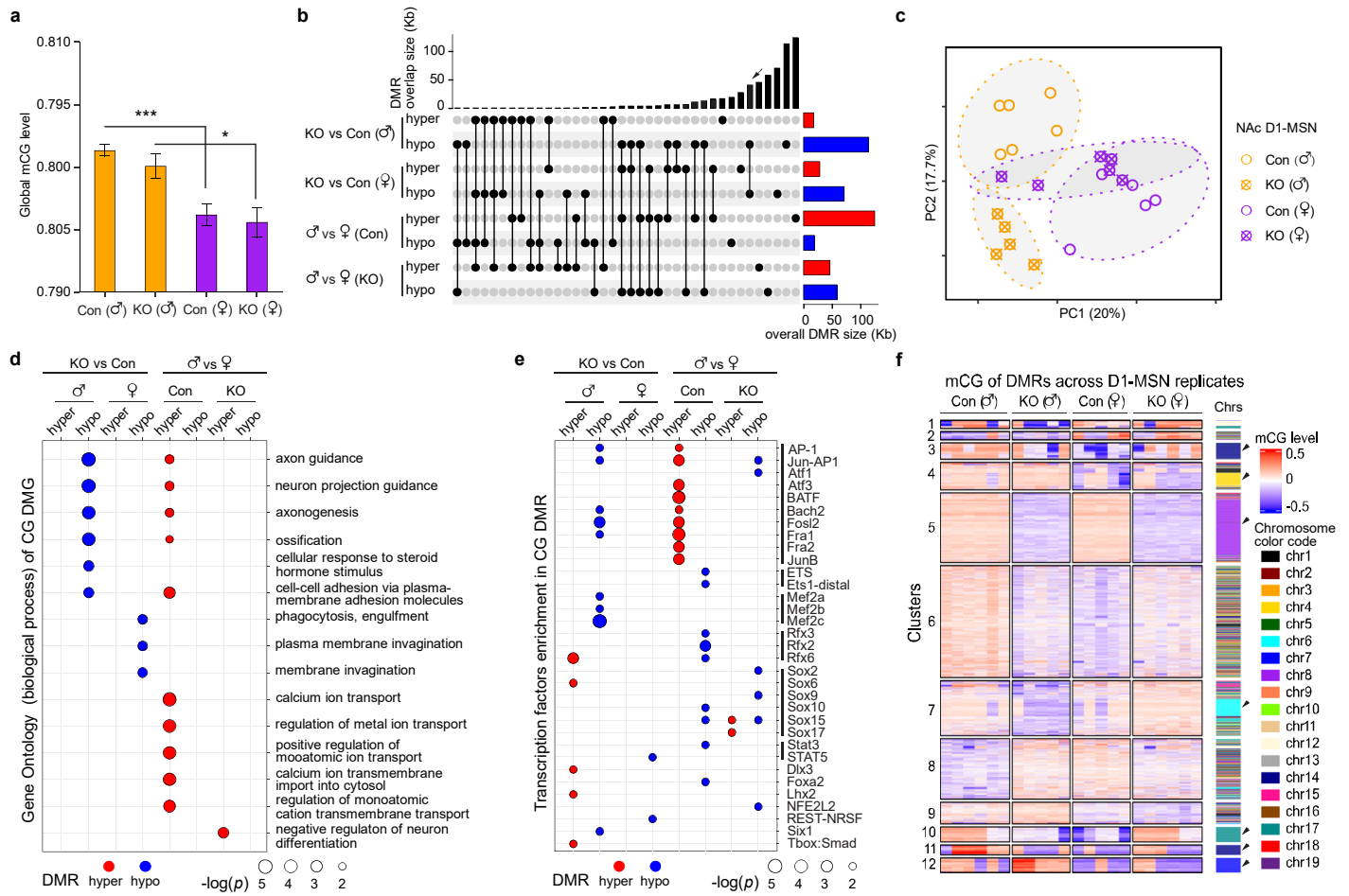


**Figure 3. Sex-specific DNA methylome changes in D1 *Tet1* KO MSNs in nucleus accumbens.** (a) Global CG methylation levels in D1-MSNs in nucleus accumbens of control (Con) and D1 *Tet1* knockout (KO) male and female mice, calculated from whole genome bisulfite sequencing. Analysis of covariance (ANCOVA) was used for the statistic test with CG conversion rate as a covariate. Sex,  $p = 0.00682$ , *Tet1*,  $p = 0.35622$ , CG conversion rate,  $p = 0.61584$ . Post hoc, two-sample t-test with Bonferroni correction ( $n=6$  for male Con,  $n = 5$  for male KO,  $n = 5$  for female Con,  $n = 6$  for female KO), \*\*\*  $p < 0.001$ , \*  $p < 0.05$ . (b) The overlaps of D1-MSN CG hyper- and hypo-DMRs across comparisons. Vertical lines connecting black dots represent overlapping DMRs in the corresponding comparisons listed on the left. The histogram on top represents the combined size of intersections. The arrow points to the most abundant overlap that existed between male “KO vs Con” hypo-DMR and female “KO vs Con” hypo-DMR. The color coded histogram on the right displays the accumulated genomic size of corresponding DMRs in each row, with hypermethylation in red and hypomethylation in blue. Number of DMRs: Male “KO vs Con” ( $n = 755$ ); female “KO vs Con” ( $n = 471$ ); control “ $\delta$  vs  $\varphi$ ” ( $n = 778$ ); *Tet1* KO “ $\delta$  vs  $\varphi$ ” ( $n = 618$ ). (c) Principal component analysis (PCA) of methylation levels of D1-MSN CG DMRs in each group. Open circles and crossed-squares represent the control and *Tet1* KO groups, respectively, with male groups in orange color and females in purple. Dashed lines circle out the clustering from the same group. (d) Gene ontology analysis of D1-MSN CG DMR-associated genes (DMGs). The detailed list is in Table 3. (e) Transcription factor motif analysis of DMR DNA sequences. The solid lines on the right highlight the TFs from the same family with similar binding sequences. The detailed list is in Table 4. (f) K-means clustering of D1-MSN CG DMRs. Each row of the heatmap represents the mCG level of one CG DMR across all WGBS replicates (in 22 columns). The columns are grouped by sex and genotype as identified on top. Chrs: the color spectrum on the right of the heatmap indicates each DMR’s chromosome location, with color code of each chromosome presented on the lower right. Arrows point to the clusters that have DMRs predominantly from the same chromosome.

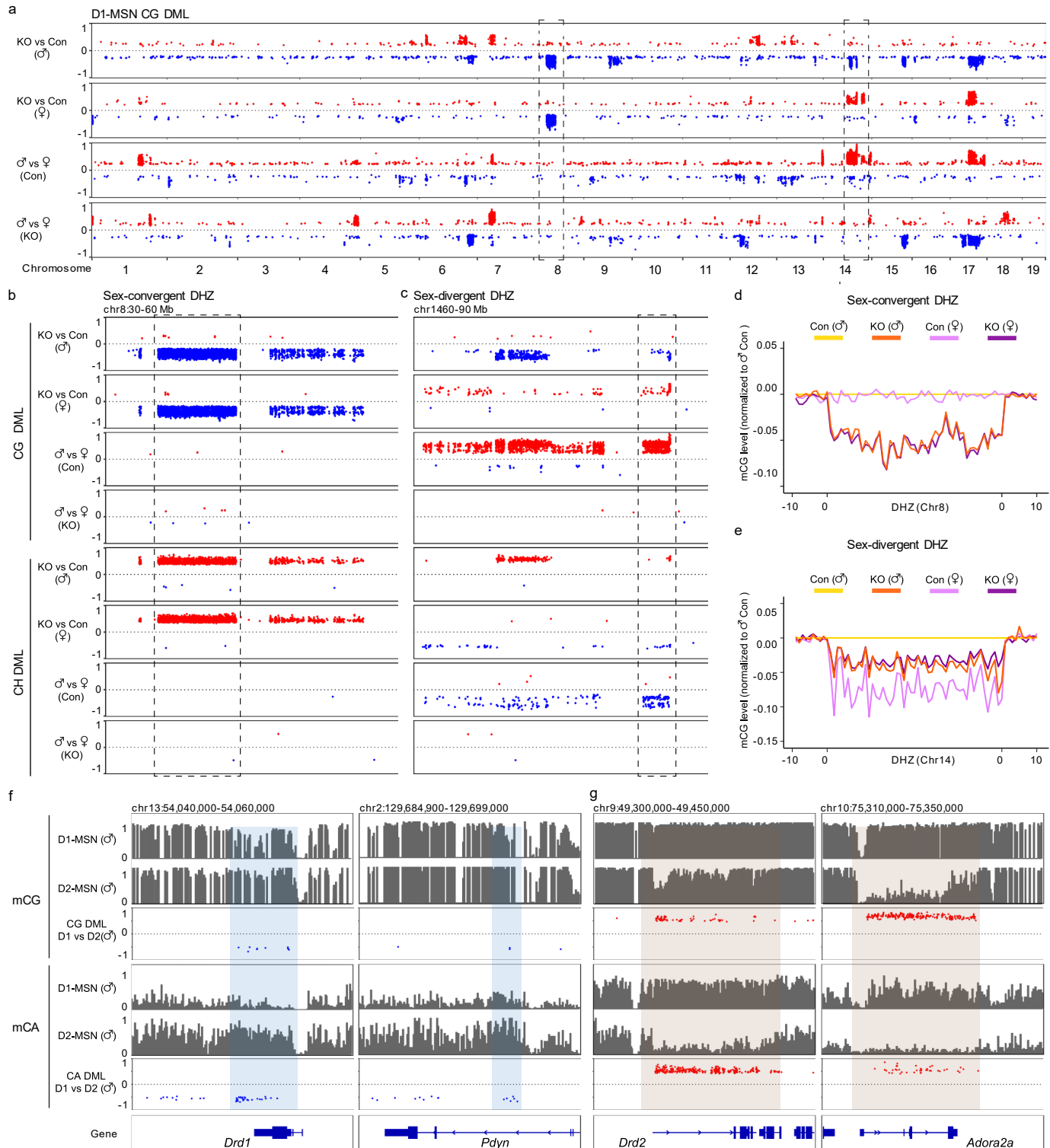


**Figure 4. TET1-dependent DNA methylation changes cluster together in a sex-specific manner.** (a) Genomic distribution of D1-MSN CG differentially methylated loci (DMLs) in each autosome. With each dot representing one DML, X-axis represents the mouse genome with chromosome names labeled and Y-axis indicates the DNA methylation difference(red: hyper-methylation, delta beta value > 0, blue: hypo-methylation, delta beta value < 0). Dashed rectangle boxes highlight one TET1-dependent sex-convergent (chr 8) and one TET1-dependent sex-divergent (chr 14) differential methylation hot zones (DHZs), where high density

differential methylation changes occur in a long stretch of DNA. Number of DMLs in each comparison: male “KO vs Con” (7,516); female “KO vs Con” (6,183); control “♂ vs ♀” (7,084); *Tet1* KO “♂ vs ♀” (5,716). The full list of CG DMLs is in Table 6. A closer view of these two representative DHZs is shown in (b) and (c), in addition to presentation of CH DMLs from the same genomic region presented at the bottom. (d) mCG levels of each sample group (normalized to the mCG levels of male control group) across the sex-convergent DHZ on chr 8 (shown in a and b), with regional loss of CG methylation after *TET1* KO in both sexes. (e) The sex-divergent DHZ on chr 14 (shown in a and c) shows opposite CG methylation change in males and females after *Tet1* KO. While the male control group exhibits high DNA methylation compared to the female control, this difference is mostly abolished after *Tet1* KO. (f) CG (top) and CA (bottom) hypomethylation at the D1-MSN marker genes *Drd1* and *Pdyn* in male D1-MSN vs male D2-MSN comparison. (g) CG (top) and CA (bottom) hypermethylation at D2-MSN marker genes *Drd2* and *Adora2a* in male D1-MSN vs male D2-MSN comparison. Shaded areas in f and g highlight the region with differential changes.

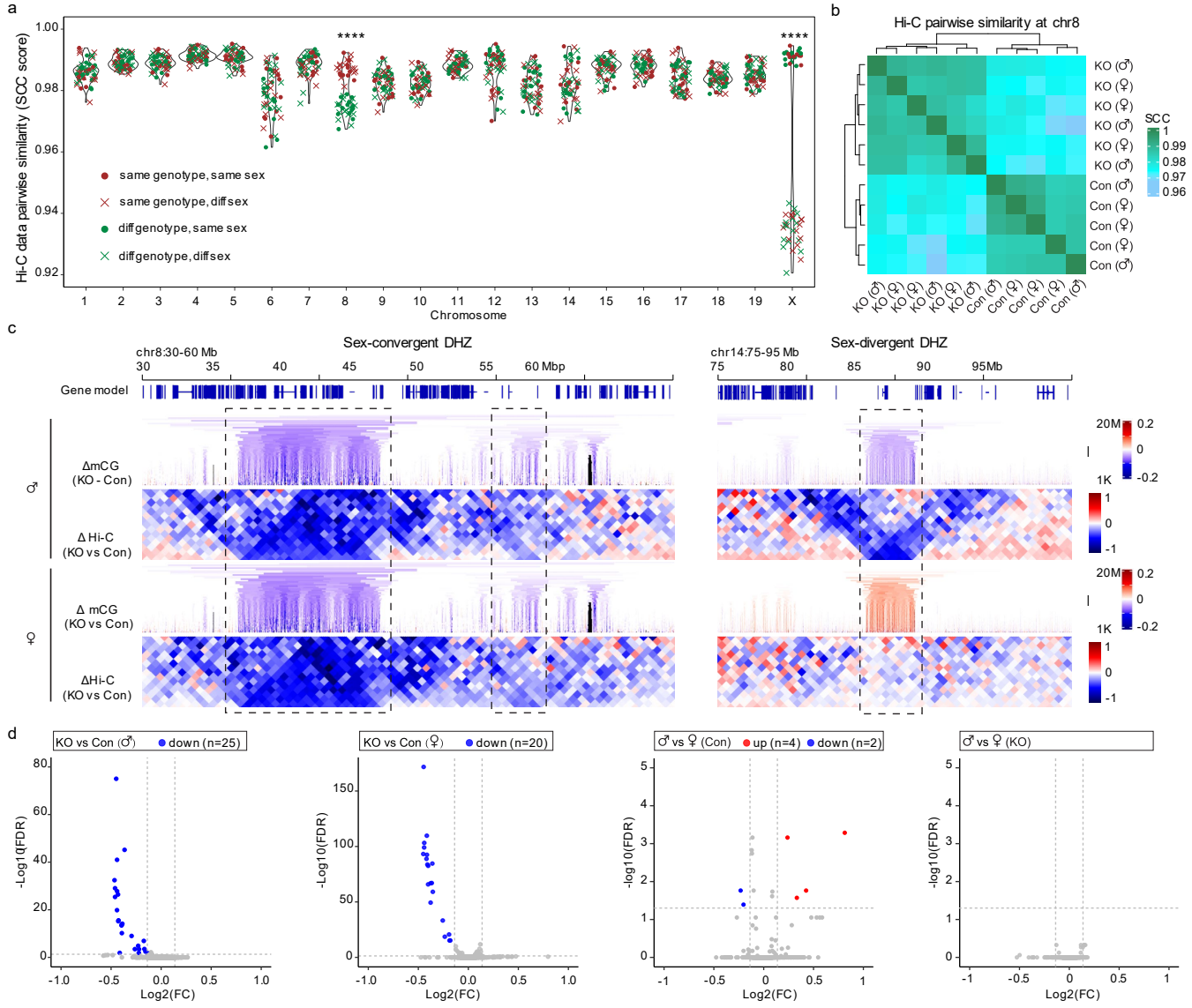


**Figure 5. TET1-dependent DNA methylation changes are associated with alterations in higher order genome organization.**

**(a)** Pair-wise comparison of individual chromosomal interaction similarities using Hi-C data. The stratum adjusted correlation coefficient (SCC) score on Y-axis is calculated using the intra-chromosomal Hi-C matrices of a pair of samples. Red dot denotes the sample pair that has the same genotype (i.e., Control (Con) or *Tet1* KO) and same sex, while red “X” represents the sample pair with the same genotype but different sex. Green dot or “X” denotes sample pair of different genotypes, but with the same sex or different sexes, respectively. Significant difference was observed at chromosomes 8 in comparison between same genotype pairs and different genotype pairs, and at X chromosome in comparison between same-sex pairs and different sexes pairs. \*\*\*\* p < 0.0001, Wilcoxon rank sum exact test (n = 25, 30).

**(b)** Pairwise similarity between Hi-C matrices based on SCC correlation scores at chromosome 8. Each row or column represents one Hi-C replicate. Their similarity clustering shows a separation between Con and *Tet1* KO.

**(c)** Chromosomal interaction changes in both sex-convergent (chr8) and sex-divergent (chr14) DHZs. “Δ mCG (KO - Con)” presents the multi-level (1 kb to 20 Mb bin sizes) CG methylation differences between KO and Con groups. “Δ Hi-C (KO vs Con)” displays the chromosomal interaction differences between read number-normalized Hi-C matrices of merged KO and Con groups at 500kb resolution. Color codes and scale bars are listed on the far right. Dashed-boxed regions highlight the concurrent 3D genome interaction differences and DNA methylation change after *TET1* KO.

**(d)** *Tet1* KO dependant differentially interacting regions (DIRs) comparing *Tet1* KO to Con groups in males, females, and sex-specific DIRs comparing male vs female in control groups, and in KO groups (from left to right). The horizontal dashed line is for FDR cutoff and the two vertical dashed lines are for up/down log2 FC.

The FC threshold is  $\pm 10\%$ . The color-coded dots (red: up, blue: down) represent DIRs that pass the cutoffs. Each dot denotes the genomic interaction within one 1.5 Mb genomic bin. The full list of DIR bins is in Table 10. Numbers of replicates: 2 in male Con, 3 in male KO, 3 in female Con, and 3 in female KO.

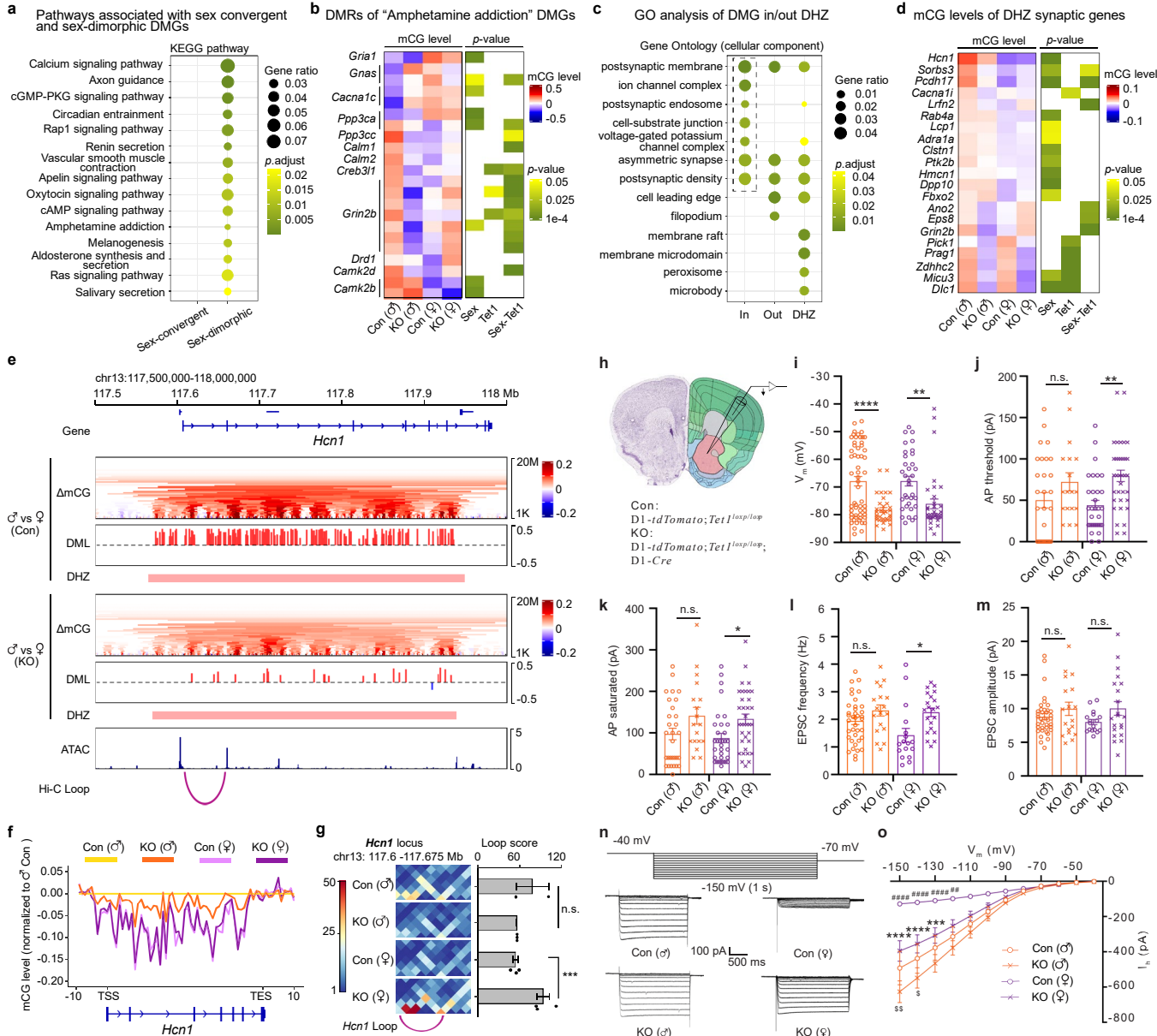
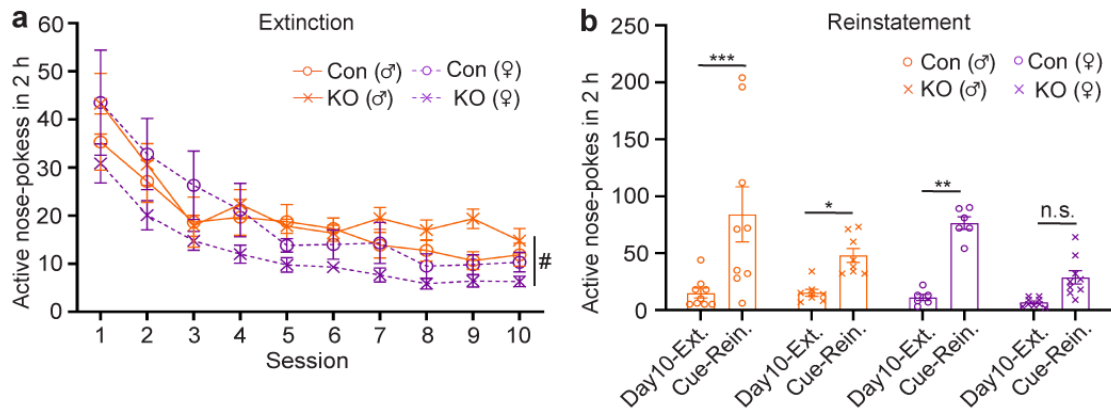
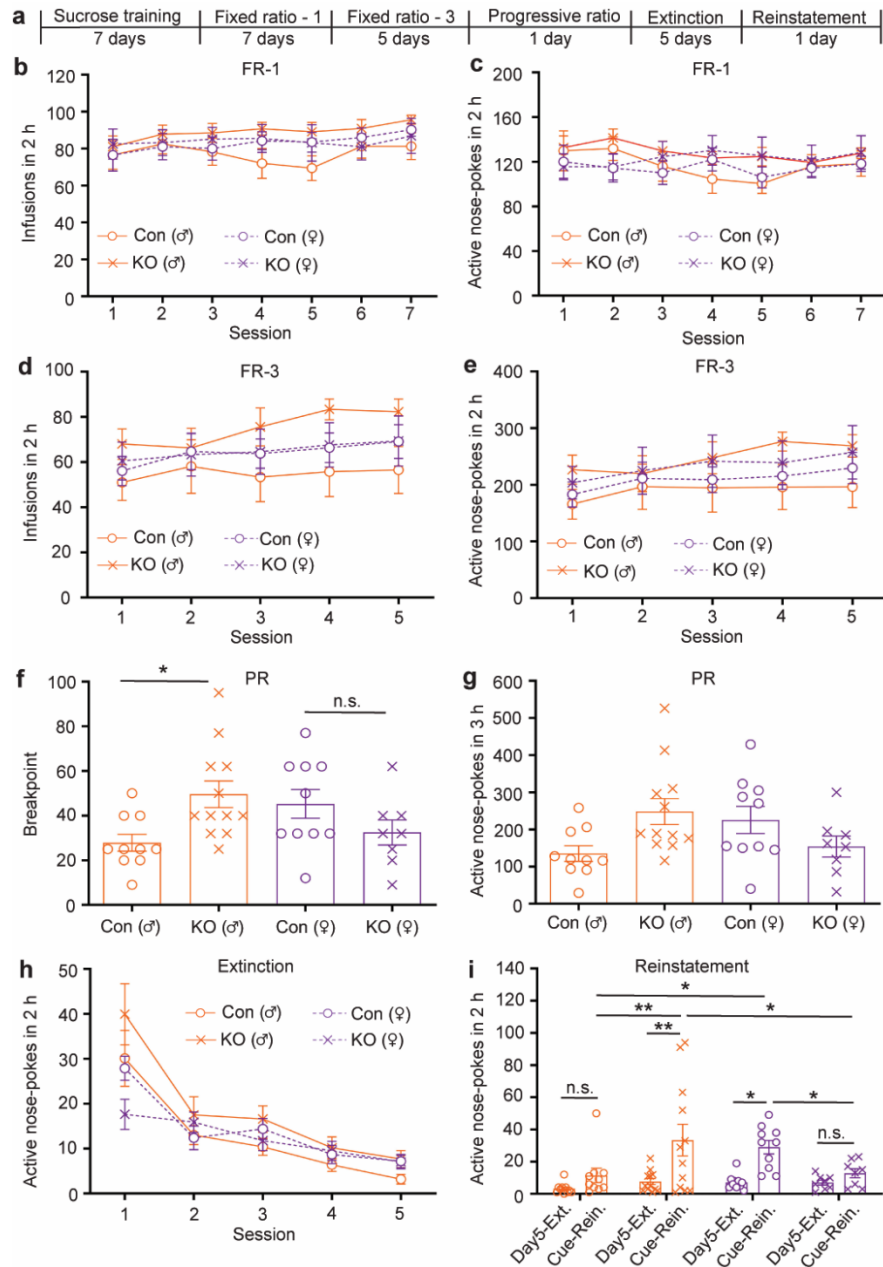


**Figure 6. Nucleus accumbens D1 *Tet1* knockout neurons are enriched with sex-specific DNA methylation changes at synaptic genes and demonstrate aberrant electrophysiological properties.** (a) Enrichment of neural function-related KEGG pathways in sex-dimorphic DMR-associated genes (DMGs), but not sex-convergent DMGs. "Gene ratio" indicates the proportion of DMGs in each pathway over the total number of genes in this pathway. (b) DMGs in "amphetamine addiction" pathway, which shows enrichment in (a). Left: A heatmap with each row represents one DMR with its normalized CG methylation levels across four groups shown. Some genes have different DMRs, therefore more rows. Right: A heatmap of significant *p*-value (two-way ANOVA,  $n = 5 - 6$ ) if the DMR is under a main effect of sex, *Tet1* KO, or their interaction (i.e., a significant sex-specific effect of

*Tet1* KO) as noted on the bottom. (c) Gene Ontology (GO) enrichment of DMGs inside DHZ, DMGs outside DHZ, and DMGs associated with a Hi-C loop located within DHZ (from left to right). Top five terms from each of the three categories are included in the figure. The complete list is in Table 13. (d) CG methylation difference across entire loci of synaptic genes in DHZ. The synaptic genes located within DHZs identified by the box-highlighted GO terms in (c). The left heatmap shows the mCG levels of the entire gene loci. The right heatmap shows the significant effect of sex, *Tet1* KO, or the sex-*Tet1* KO interaction on the mCG levels. (e) TET1-modulated sex-dimorphic DNA methylation in an exemplary gene *Hcn1* (*hyperpolarization activated cyclic nucleotide gated potassium channel 1*). From the top to the bottom: “Δ mCG” shows the multi-level (1k to 20M bin-sizes) CG methylation beta value differences between male vs female in either control or KO groups; “DML” tracks show the sex-specific CG DMLs cluster in a DHZ region, which are mostly abolished after *Tet1* KO; “DHZ” highlights the DHZ region; “ATAC” track show the ATAC-seq chromatin accessibility peaks in striatum D1-MSNs<sup>1</sup>; “Hi-C Loop” displays a chromatin interaction peak that connects two ATAC-seq peaks near *Hcn1* promoter. (f) The sex-specific CG methylation difference across *Hcn1* gene in control and *Tet1* KO. The mCG levels of *Hcn1* locus in four groups of D1-MSN are presented. (g) Increased chromatin interaction at *Hcn1* Hi-C loop (the same loop in e) in female *Tet1* KO, but not in male KO. Left: 10kb-resolution Hi-C heatmaps covering the *Hcn1* promoter loop region are presented. Right: Increased chromosomal interaction of *Hcn1* Hi-C loop is observed in all three female *Tet1* KO replicates, but not males, in comparison to their respective control. N = 2 – 3. \*\*\* adjusted.p < 0.001. (h) Electrophysiological recordings in D1-tdTomato; *Tet1*<sup>lloxP/lloxP</sup> (control) and D1-tdTomato; D1Cre (+); *Tet1*<sup>lloxP/lloxP</sup> (KO) mice in which NAc D1-MSNs can be visualized by the expression of tdTomato. (i) Resting membrane potentials of NAc D1-MSNs. Genotype (F1, 156 = 29.60, p < 0.0001). Number of cells recorded: Con ♂: 57, KO ♂: 34, Con ♀: 34 and KO ♀: 35. (j) The threshold stimulus (current injection) required for AP initiation. Genotype (F1, 112 = 12.32, p = 0.0006). (k) The saturated stimulus for AP production. Genotype (F1, 112 = 10.15, p = 0.0019). Number of cells recorded: Con ♂: 30, KO ♂: 18, Con ♀: 33, and KO ♀: 35. \* p < 0.05, \*\* p < 0.01. (l) EPSC frequency (Genotype, F1, 90 = 11.09, p = 0.0013) and (m) amplitude of NAc D1-MSNs, respectively. Number of cells recorded: Con ♂: 38, KO ♂: 18, Con ♀: 17 and KO ♀: 21. \* p < 0.05. (n) Voltage protocol for evoking hyperpolarization-activated currents (I<sub>h</sub>) and representative traces showing I<sub>h</sub> currents recorded on NAc D1-MSNs of each group. (o) Current-voltage relationship of I<sub>h</sub> currents. Number of cells recorded: Con ♂: 12, KO ♂: 9, Con ♀: 16 and KO ♀: 19. KO (♀) vs Con (♀), \*\*\* p < 0.001, \*\*\*\* p < 0.0001; Con (♀) vs Con (♂), # p < 0.05, ## p < 0.01, ### p < 0.001, and ##### p < 0.0001; KO (♀) vs KO (♂), \$ p < 0.05, \$\$, p < 0.01. Data are presented as mean ± SEM. n.s., no significance.

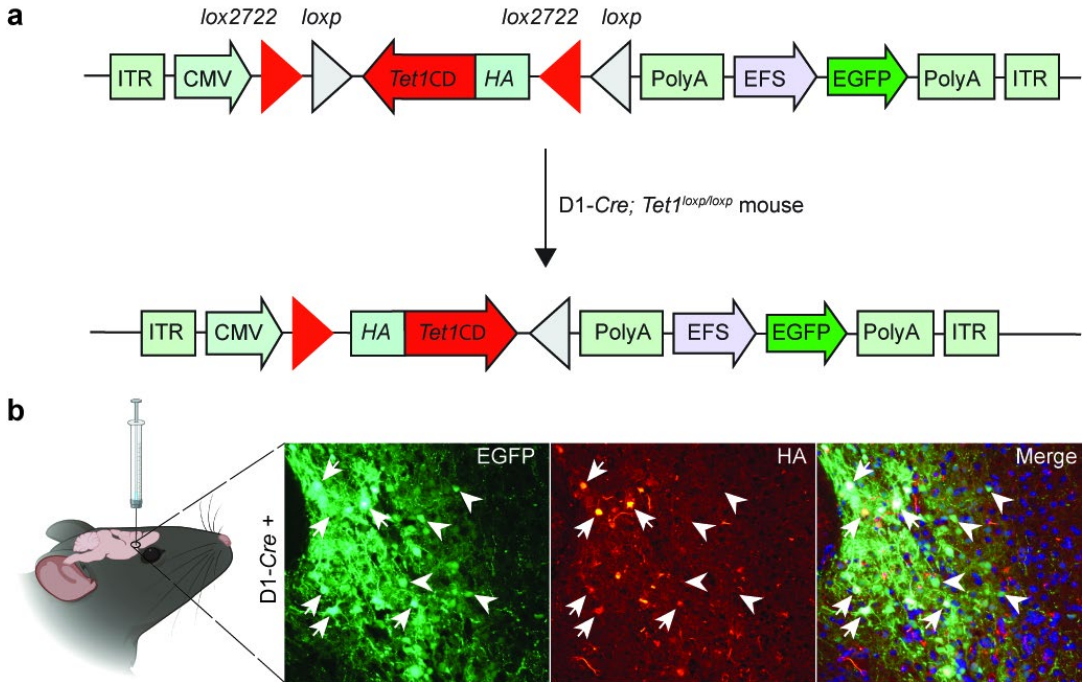


**Extended Data Figure 1. Sex specific roles of TET1 in cocaine extinction and cue-induced reinstatement.** (a) Number of active nose-pokes across 10 days of extinction. Three-way repeated-measures ANOVA, session ( $F_{9, 279} = 32.6, p < 0.0001$ ), sex ( $F_{1, 31} = 4.506, p = 0.0419$ ) and #, sex × genotype ( $F_{1, 31} = 6.725, p = 0.0144$ ). n = 6 - 11. (b) Number of active nose-pokes during cue-induced reinstatement of cocaine seeking. Three-way ANOVA, session ( $F_{1, 56} = 39.04, p < 0.0001$ ), genotype ( $F_{1, 56} = 8.378, p = 0.0054$ ), and session × genotype ( $F_{1, 56} = 6.923, p = 0.0110$ ). n.s., no significance, \*  $p < 0.05$ , \*\*  $p < 0.01$ , and \*\*\*  $p < 0.001$ . n = 6 - 9. Data are presented as mean ± SEM. Con: control; KO: D1-Tet1 KO; Ext., extinction; Rein., reinstatement.

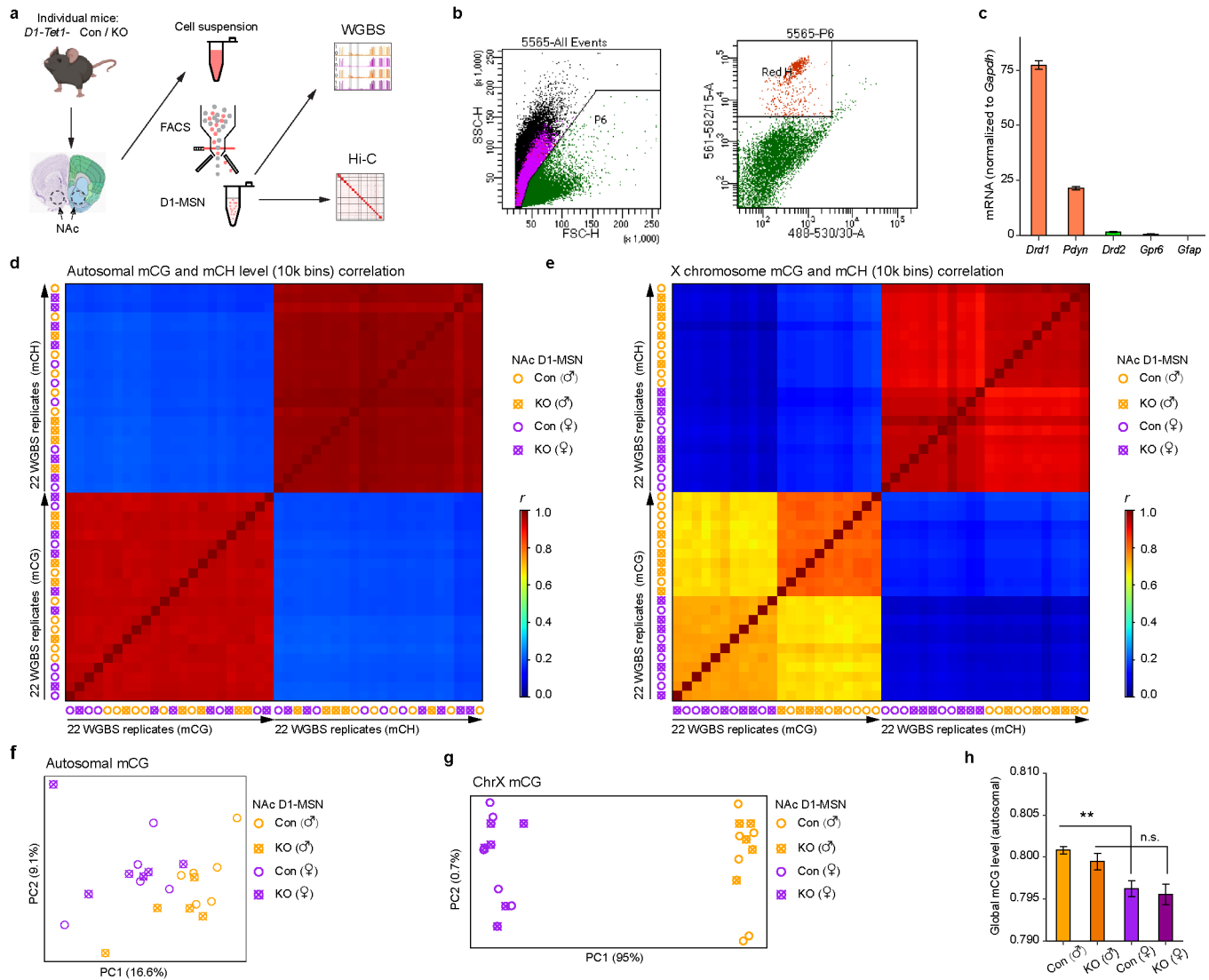


**Extended Data Figure 2. Sex specific roles of TET1 in sucrose self-administration, extinction, and cue-induced reinstatement.**

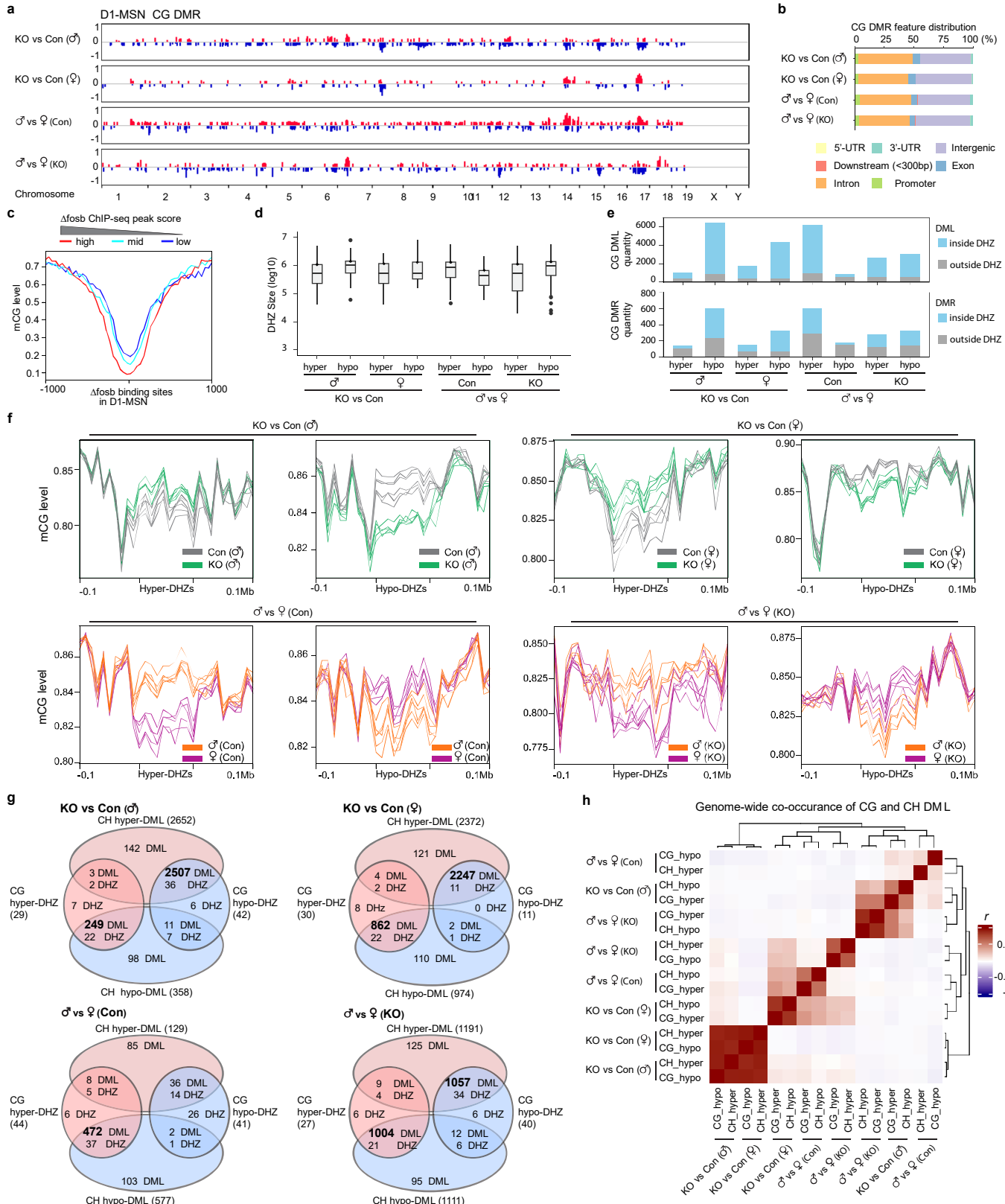
(a) Schematic timeline of sucrose self-administration behavioral testing procedure. (b) Number of sucrose intakes under fixed ratio-1 (FR-1) schedule. Session ( $F_{6, 216} = 2.5$ ,  $p = 0.0233$ ). (c) Number of active nose-pokes under FR-1. Three-way repeated-measures ANOVA, no significant main effects found. (d) Number of sucrose intakes under fixed ratio-3 (FR-3) schedule. Three-way repeated-measures ANOVA, session ( $F_{4, 144} = 4.50$ ,  $p = 0.0019$ ). (e) Number of active nose-pokes under FR-3. Three-way repeated-measures ANOVA, session ( $F_{4, 144} = 5.044$ ,  $p = 0.0008$ ). (f) Breakpoints earned under progressive ratio (PR) schedule. Two-way ANOVA, sex  $\times$  genotype ( $F_{1, 36} = 9.166$ ,  $p = 0.0045$ ), \*  $p < 0.05$ . (g) Active nose-pokes under PR. Two-way ANOVA, sex  $\times$  genotype ( $F_{1, 36} = 8.261$ ,  $p = 0.0068$ ). (h) Number of active nose-pokes across 5 days of extinction of sucrose seeking. Three-way repeated measures ANOVA, session ( $F_{4, 144} = 42.1$ ,  $p < 0.0001$ ). (i) Active nose-pokes during reinstatement test. Three-way ANOVA, session ( $F_{1, 72} = 18.85$ ,  $p < 0.0001$ ), sex  $\times$  genotype ( $F_{1, 72} = 9.178$ ,  $p = 0.0034$ ), and session  $\times$  sex  $\times$  genotype ( $F_{1, 72} = 5.616$ ,  $p = 0.0205$ ), \*  $p < 0.05$  and \*\*  $p < 0.01$ .  $n = 8 - 12$ . Data are presented as mean  $\pm$  SEM. Con: control; KO: D1-Tet1 KO; Ext., extinction; Rein., reinstatement.



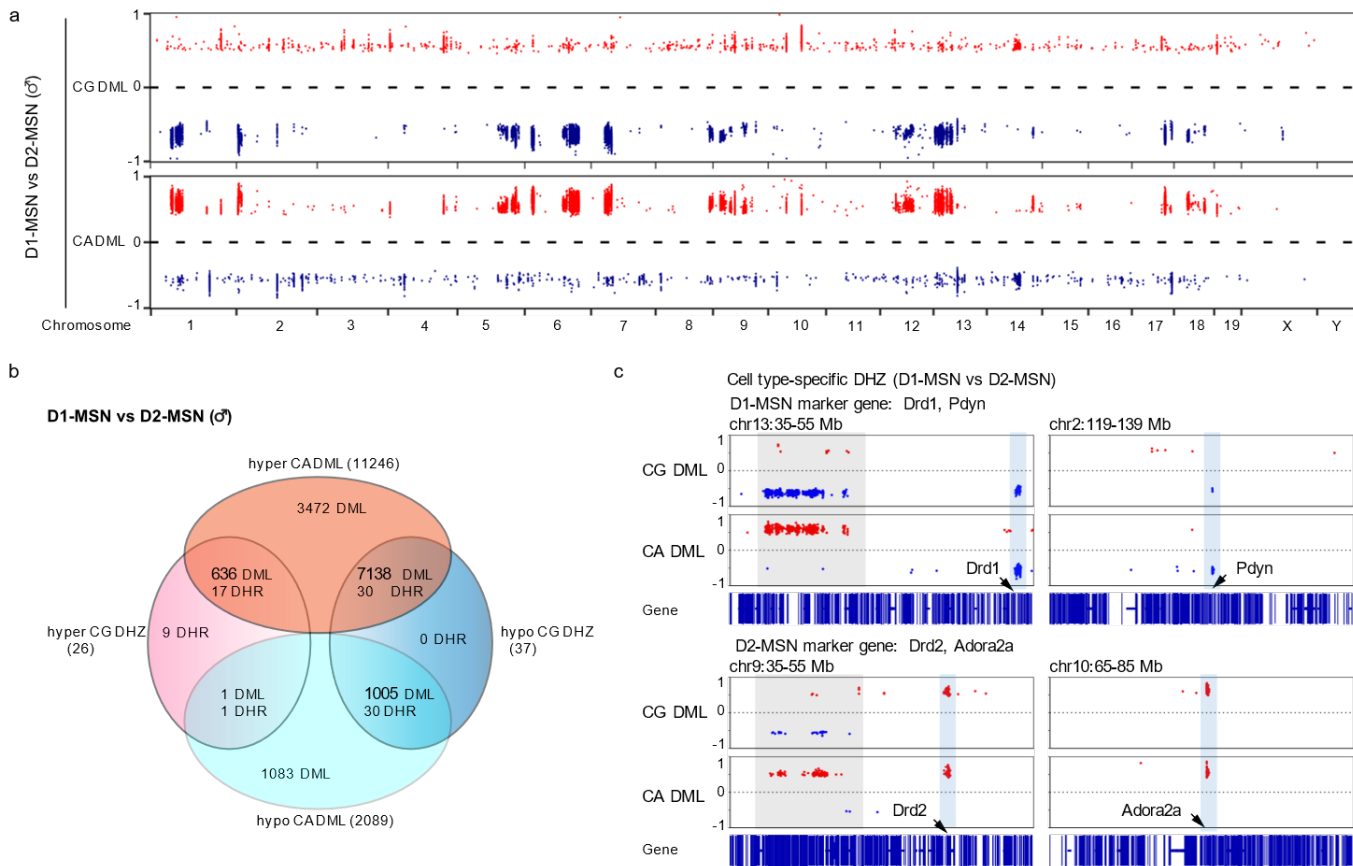
**Extended Data Figure 3. Viral-mediated TET1 overexpression in mouse nucleus accumbens D1-medium spiny neurons.** (a) AAV2 viral vector construct of Cre-recombinase dependent expression of *Tet1* catalytic domain (*Tet1CD*). By using the FLEX-on design, the HA-*Tet1CD* fusion is reversely inserted downstream to a CMV promoter in between interlocking pairs of lox 2272 and loxP sites. An EGFP coding sequence was added outside of the loxP sites for expression inspection. The mutant *Tet1* CD (two-point mutations in TET1 CD sequence) was applied to replace the *Tet1* wildtype (wt*Tet1CD*) in the *Tet1* mutant (mut*Tet1CD*) construct (not shown). (b) Validation of Cre-dependent AAV-*Tet1CD* expression. Viral vectors are injected into the nucleus accumbens of *D1-Cre; Tet1*<sup>loxP/loxP</sup> mice. The viral infected neurons can be conveyed by green signals of EGFP expression. Cre dependent expression of HA signal can be recognized in D1 neurons. Therefore, the colocalization of HA and EGFP represent Cre expressing D1-neurons (e.g., pointed by arrows), and EGFP expression without HA indicate viral infected neurons without D1 expression (e.g., pointed by arrowheads).



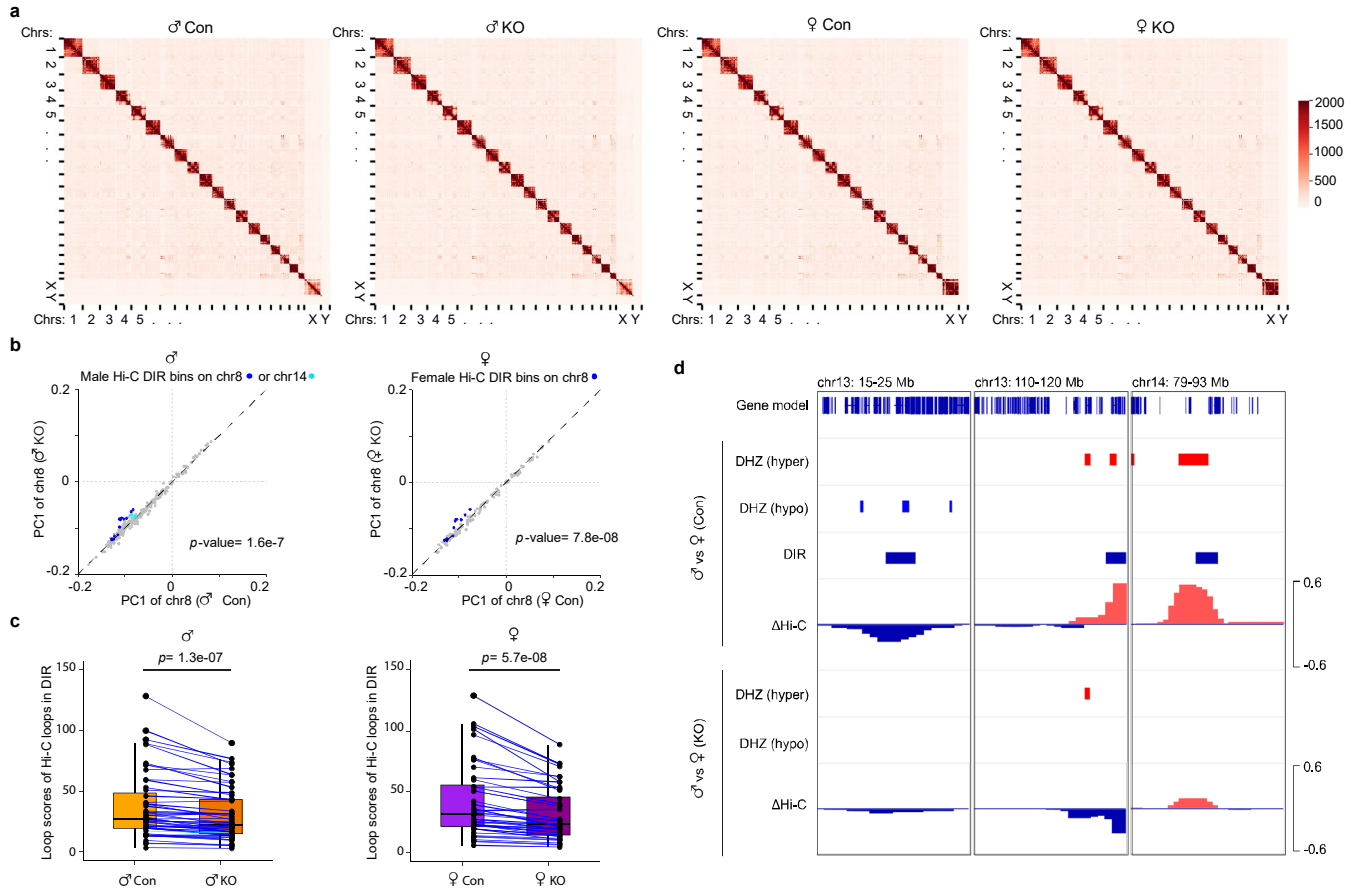
**Extended Data Figure 4. Nucleus accumbens D1 medium spiny neuron isolation and whole-genome DNA methylation profiling.** (a) A schematic experimental procedure of D1-medium spiny neuron (D1-MSN) isolation by fluorescence-activated cell sorting (FACS) from the nucleus accumbens (NAc) of D1-cre (+); *Tet1*<sup>loxP/loxP</sup>; D1-tdTomato mice (KO) or *Tet1*<sup>loxP/loxP</sup>; D1-tdTomato mice (Con), and the subsequent epigenomic profiling (WGBS: whole-genome bisulfite sequencing. Hi-C: chromosome conformation capture). (b) Representative D1-MSN FACS plots. Left: all FACS events using FSC-H and SSC-H gating. Right: A population with “Red H” signal is collected under 488-530/30-A and 561-582/15-A fluorescence gating. (c) qPCR analysis of FACS isolated D1-MSNs confirms the transcription enrichment of D1-MSN marker genes (*Drd1*, *Pdyn*), but not marker genes of D2-MSNs (*Drd2*, *Gpr6*), or astrocytes (*Gfap*). All are normalized to *Gapdh*. n = 4 for each gene. (d-e) Pair-wise correlation of CG and CH methylation levels of autosomes (d) and X chromosomes (chrX) (e). The analysis is done in 100kb bins across all four groups (con and KO of both sexes) of all replicates (n=22). There are high correlations among all replicates in autosomal levels of methylated CG (mCG), or mCH(d). The X chromosome CG and CH methylation levels are better correlated within groups of the same sex (e). “r”, Pearson correlation coefficient. (f-g) PCA analysis of genome-wide autosomal (h), and X chromosome mCG levels (i) across four groups of D1-MSNs, utilizing 100 kb bins. (h) Global autosomal mCG levels of male and female D1-MSNs. Analysis of covariance (ANCOVA) was used for the statistic test with CG conversion rate as a covariate. Sex, p = 0.0189, Tet1, p = 0.3366, CG conversion rate, p = 0.6267. Post hoc, two-sample t-test with Bonferroni correction. \*\* p < 0.01, n.s.: no significance.



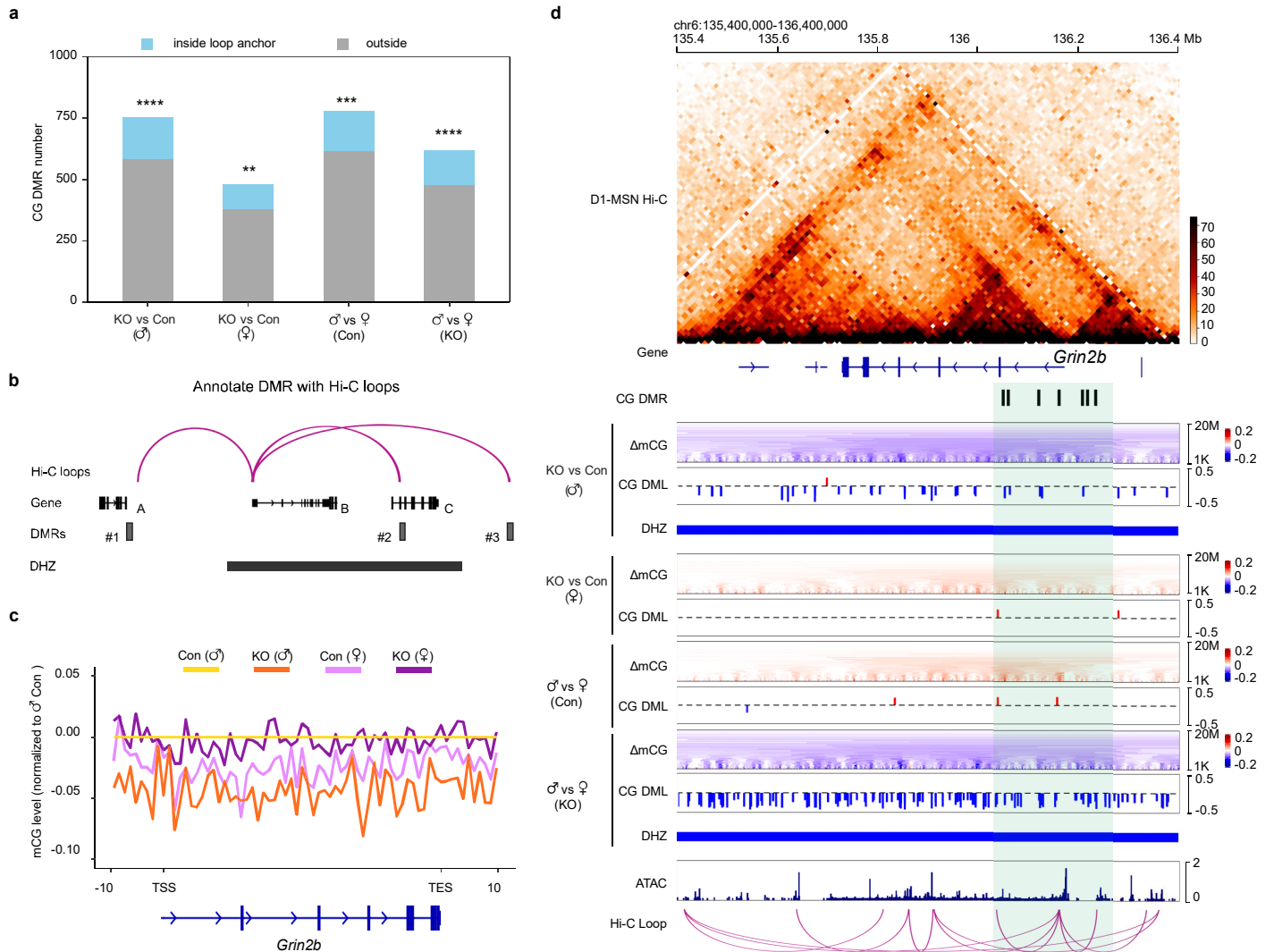
**Extended Data Figure 5. Differential methylation hot zones (DHZs) are characterized by high-frequency same direction of DNA methylation changes in a long genomic region.** (a) Genome-wide distribution of D1-MSN CG differential methylation regions (DMRs). KO vs Con (♂): DMRs comparing male *Tet1* KO to male control; KO vs Con (♀): DMRs comparing female *Tet1* KO to female control; ♂ vs ♀ (Con): DMRs comparing male control to female control; ♂ vs ♀ (KO): DMRs comparing male *Tet1* KO to female *Tet1* KO. Red: hyper-methylation DMRs, blue: hypo-methylation DMRs. (b) Genomic feature distribution of CG DMRs. 5'-UTR: five prime untranslated region. 3'-UTR: three prime untranslated region. Intergenic: distal intergenic region. Downstream: 300 bp downstream the gene 3'-UTR region. Promoter: -1000 to +100 bp regions of transcription starting site (TSS). (c) The reverse-correlation between DNA methylation levels and ΔFosB enrichments. The averaged CG methylation levels within the upstream 1000 bp to downstream 1000 bp region of the top, middle, and bottom 1000 ΔFosB enrichment sites are reflected in three separate traces (ChIP-seq peaks retrieved from a published dataset<sup>2</sup>). (d) The combined genomic sizes of hyper- and hypo-DHZs in each of the four comparisons. (e) Quantities of CG DMLs (top) and CG DMRs (bottom) that are located inside (blue color) or outside (grey color) a DHZ. (f) The accumulative plots of DHZ mCG level shows that both TET1-dependant and sex-specific DHZs exhibit pervasive hyper- or hypo-methylation. Every trace in each plot represents the aggregated DNA methylation in corresponding DHZs in one replicate (DNA methylome of the NAc D1-MSN from one mouse). (g) Overlapping between CH DMLs and CG DHZs. Most CH DMLs overlap with CG DHZs identified from CG DMLs. Numbers indicate the count of DMLs or DHZs. Bold numbers represent the most abundant overlapping between CH DMLs and CG DHZs, which all have opposing directions of methylation changes. (h) CG and CH DML density correlation analysis shows genome-wide co-occurrence between CH DMLs and CG DMLs. Higher correlations exist between CG hypo-DMLs and CH hyper-DMLs, or between CG hyper-DMLs and CH hypo-DMLs. “r”, pearson correlation coefficient.



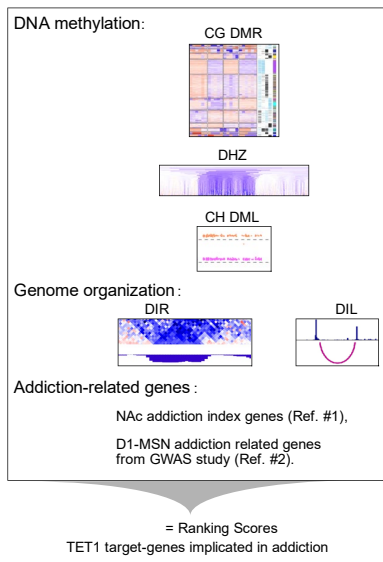
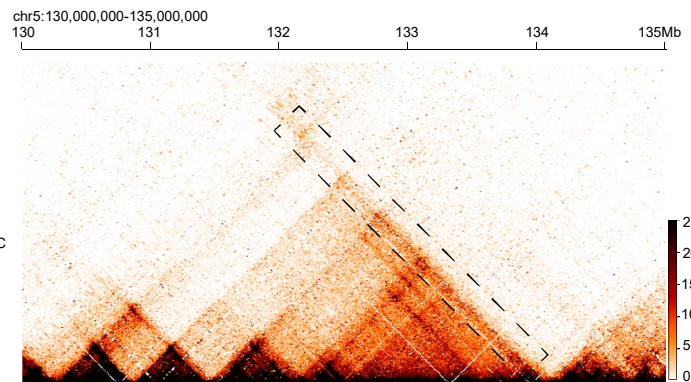
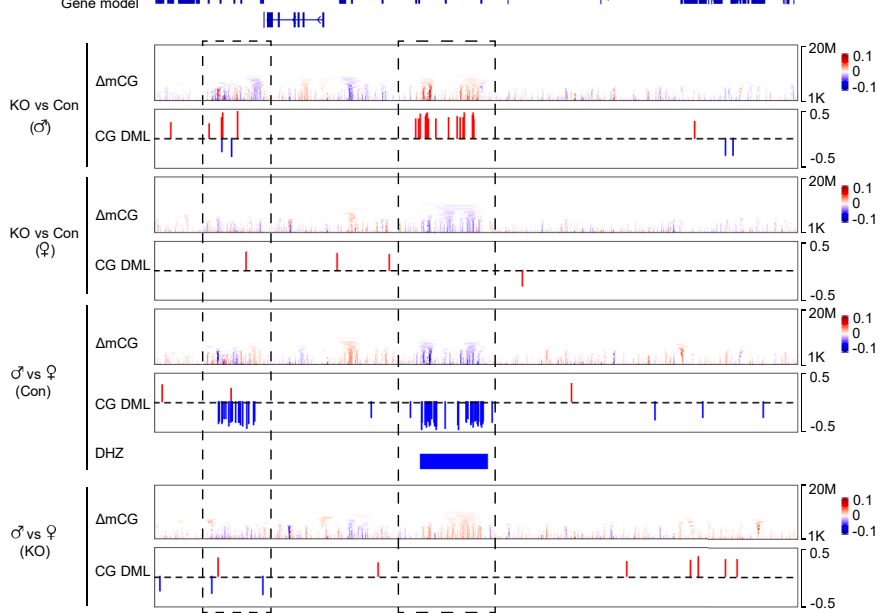
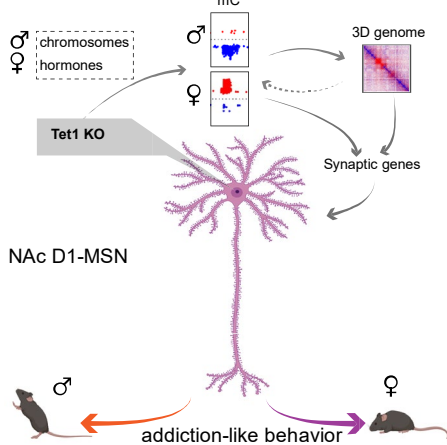
**Extended Data Figure 6. NAc MSN cell type-specific DHZs.** (a) Genome-wide chromosomal distribution of CG and CH (represented by CA) DMLs by comparing NAc D1-MSN and D2-MSN in males. The distribution pattern of CG hypo-DMLs (in blue) and CH hyper-DMLs (in red) appear to mostly mirror each other. (b) Co-localization of cell type-specific CH DMLs (compare male D1-MSN vs male D2-MSN) with CG DHZs. The three bold numbers indicate a significant portion of overlap. (c) Cell type-specific DHZs (compare male D1-MSN vs male D2-MSN) show same directions of CH and CG methylation changes in D1-MSN and D2-MSN marker genes. For example, hypomethylated CG DMLs and CH DMLs are co-localized at D1 neuron marker genes *Drd1*, *Pdyn* (light blue shaded areas in top two panels), while DHZs at D2 neuron marker genes *Drd2*, *Adora2a* show hypermethylated CG DMLs and CH DMLs (light blue shaded areas in bottom two panels). In contrast, the neighboring DHZs away from D1 marker gene *Drd1* and D2 marker gene *Drd2* (grey color shaded areas in the two left panels) demonstrate opposite directions of methylation changes in CG DMLs and CH DMLs. Arrows point out the approximate location of respective genes.



**Extended Data Figure 7. Characterization of 3D genome interactions in D1-MSNs.** (a) Genome-wide Hi-C contact heatmap for the four groups (male control, male *Tet1* KO, female control, female *Tet1* KO). Color code annotated on top right reflects the chromosome interaction score. (b) The PC1 value of Hi-C A/B compartmental analysis is elevated in DIRs in *Tet1* KO in both males (left) and females (right). *P*-values were calculated between the PC1 value of DIR significant bins and other bins on chr8 and chr14 by two-way Z-tests for males ( $z = -5.2396$ ,  $p$ -value =  $1.6e-07$ ) and chr8 for females ( $z = -5.37$ ,  $p$  =  $7.87e-08$ ), respectively.  $n = 15$  (male, inside), 240 (male, outside), 12 (female, inside), 118 (female outside). Genomic bins in DIRs on chr8 are colored blue, and two bins in the chr14 DIR are colored cyan. (c) The lower loop score in DIRs in *Tet1* KO males (left) and females (right) indicating attenuated 3D looping interaction. *P*-values were calculated by paired t-tests (males:  $n = 51$ ,  $Df = 50$ ,  $t = -6.142$ ,  $p = 1.3e-07$ ; females:  $n = 44$ ,  $Df = 43$ ,  $t = -6.5562$ ,  $p = 5.7e-08$ ). Most loops in DIRs on chr8 are colored blue, with one loop in chr14 DIR in male groups colored cyan (left panel). (d) Sex-specific ( $\delta$  vs  $\varphi$ ) genome interaction alterations (DIR) overlap with sex-specific CG methylation changes (DHZ). Representative cases in chr 13 and chr 14 are shown. Both DIRs and DHZs appear to be abolished in *Tet1* KO.  $\Delta$ Hi-C: log<sub>2</sub> fold change of male to female Hi-C genome interaction comparison in 1.5Mb genomic bins.



**Extended data Figure 8. Integration of DNA methylation changes and Hi-C loops.** (a) CG DMRs are enriched in D1-MSN Hi-C loop anchor regions. Fisher's exact tests were performed using the “bedtools fisher” tool. \*\*:  $p < 0.01$ , \*\*\*:  $p < 0.001$ , \*\*\*\*:  $p < 0.0001$ . D1-MSN Hi-C loops are available in Table 11. (b) A schematic representation of DMR gene annotations. In addition to annotate DMRs to their proximate genes (e.g. DMR #1 to gene A, DMR #2 to gene C), distal DMRs (#1, #2, #3 relative to gene B) are also assigned to Hi-C loop connected target genes (gene B here). The full list of D1-MSN Hi-C loops is in Table 11. Similarly, DHZ loop genes were retrieved for the GO analysis in Figure 6c. (c) The mCG level at *Grin2b* gene locus decreases in *Tet1* KO males, but increases in KO females, indicating an interaction effect of sex and TET1 on DNA methylation. (d) *Grin2b* is located in a sex-specific and TET1-dependent DHZ. From the top to the bottom, “D1-MSN Hi-C” displays a Hi-C interaction heatmap at 10kb resolution; “CG DMR” illustrates DMRs assigned to *Grin2b* based on Hi-C loops and linear proximity to TSS; “ $\Delta$  mCG” plots depict the multilevel (1 k to 20 M bin sizes) CG methylation beta value differences between groups; “CG DML” plots are the DMLs of corresponding comparisons; “ATAC” shows the chromatin accessibility peaks of striatum D1-MSN; “Hi-C Loop” displays the chromatin interaction peaks. The shaded area across all traces highlights the region containing sex dimorphic CG DMRs (listed in Fig. 6b) located proximate to the *Grin2b* Hi-C loop anchors and ATACseq open chromatin regions.

**a****b**Gene model  
*Caln1*      *Auts2***c**

**Extended data Figure 9. Identification of addiction associated D1-MSN TET1 target genes.** (a) The schematic workflow to predict TET1 target genes in NAc D1-MSNs that may function in drug addiction. TET1 target genes are the combination of genes associated with DNA methylation changes (including CG DMRs, DHZs, CH DMLs), and/or genome organizational alterations (DIRs and DILs). They were then prioritized through an integration with two addiction-related gene lists that include NAc addiction index genes<sup>3</sup> (Ref. #1), and D1-MSN addiction-related genes from a cell type-specific GWAS study<sup>4</sup>. DILs, differentially interacting loops. (b) Chromosome structure and DNA methylation based connection between two addiction related genes *Auts2* and *Caln1*. In D1-MSN, the chromatin interaction between these two gene loci is reflected in a “stripe”-like interaction pattern (dashed rectangles on the upper panel), which indicates the genomic region near chr5:134Mb interacts frequently with multiple consecutive regions along the left side chromosome including both *Caln1* and *Auts2* gene loci). In addition, *Auts2* and *Caln1* exhibit synchronized DNA methylation dynamics across one DHZ and one DHZ-like regions (dashed rectangles on genome tracks of the lower panels). These two regions both show hyper-DML in male *Tet1* KO (KO vs Con ( $\delta$ )) and hypo-methylation comparing control males to control females ( $\delta$  vs  $\varphi$  (Con)). (c) A schematic presentation of TET1 targets synaptic genes in NAc D1-MSNs, which can be modulated by DNA methylation and higher order genome organization to regulate drug addiction-like behaviors in a sex-specific manner.

## References

- 1 Li, Y. E. *et al.* An atlas of gene regulatory elements in adult mouse cerebrum. *Nature* **598**, 129-136, doi:10.1038/s41586-021-03604-1 (2021).
- 2 Yeh, S. Y. *et al.* Cell Type-Specific Whole-Genome Landscape of DeltaFOSB Binding in the Nucleus Accumbens After Chronic Cocaine Exposure. *Biol Psychiatry* **94**, 367-377, doi:10.1016/j.biopsych.2022.12.021 (2023).
- 3 Walker, D. M. *et al.* Cocaine Self-administration Alters Transcriptome-wide Responses in the Brain's Reward Circuitry. *Biol Psychiatry* **84**, 867-880, doi:10.1016/j.biopsych.2018.04.009 (2018).
- 4 Srinivasan, C. *et al.* Addiction-Associated Genetic Variants Implicate Brain Cell Type- and Region-Specific Cis-Regulatory Elements in Addiction Neurobiology. *J Neurosci* **41**, 9008-9030, doi:10.1523/JNEUROSCI.2534-20.2021 (2021).